

1 SEARCH FOR PRODUCTION OF A HIGGS BOSON AND A SINGLE TOP  
2 QUARK IN MULTILEPTON FINAL STATES IN  $pp$  COLLISIONS AT  $\sqrt{s} = 13$   
3 TeV.

4 by

5 Jose Andres Monroy Montañez

# A DISSERTATION

7 Presented to the Faculty of

8 The Graduate College at the University of Nebraska

9 In Partial Fulfilment of Requirements

10 For the Degree of Doctor of Philosophy

11 Major: Physics and Astronomy

12 Under the Supervision of Kenneth Bloom and Aaron Dominguez

13 Lincoln, Nebraska

14 July, 2018

15 SEARCH FOR PRODUCTION OF A HIGGS BOSON AND A SINGLE TOP  
16 QUARK IN MULTILEPTON FINAL STATES IN pp COLLISIONS AT  $\sqrt{s} = 13$   
17 TeV.

18 Jose Andres Monroy Montañez, Ph.D.

19 University of Nebraska, 2018

20 Adviser: Kenneth Bloom and Aaron Dominguez

# **21 Table of Contents**

<b>22 Table of Contents</b>	<b>iii</b>
<b>23 List of Figures</b>	<b>vi</b>
<b>24 List of Tables</b>	<b>viii</b>
<b>25 1 INTRODUCTION</b>	<b>1</b>
<b>26 2 Theoretical approach</b>	<b>2</b>
27     2.1 Introduction . . . . .	2
28     2.2 Standard model of particle physics . . . . .	5
29         2.2.1 Fermions . . . . .	7
30             2.2.1.1 Leptons . . . . .	8
31             2.2.1.2 Quarks . . . . .	10
32         2.2.2 Fundamental interactions . . . . .	14
33         2.2.3 Gauge Bosons . . . . .	19
34     2.3 Electroweak unification and the Higgs mechanism . . . . .	21
35         2.3.1 Spontaneous symmetry breaking . . . . .	29
36         2.3.2 Higgs mechanism . . . . .	33
37         2.3.3 Masses of the gauge bosons . . . . .	35

38	2.3.4	Masses of the fermions . . . . .	36
39	2.3.5	The Higgs field . . . . .	37
40	2.3.6	Higgs boson production mechanisms at LHC. . . . .	38
41	2.3.7	Higgs decay channels . . . . .	42
42	2.4	Associated Production of Higgs Boson and Single Top Quark. . . . .	43
43	2.5	The CP-mixing phase . . . . .	48
44	<b>3</b>	<b>The CMS experiment at the LHC</b>	<b>49</b>
45	3.1	Introduction . . . . .	49
46	3.2	The LHC . . . . .	50
47	3.3	The CMS experiment . . . . .	54
48	<b>4</b>	<b>Search for production of a Higgs boson and a single top quark in multilepton final states in pp collisions at <math>\sqrt{s} = 13</math> TeV</b>	<b>56</b>
50	4.1	Introduction . . . . .	56
51	4.2	Data and MC Samples . . . . .	58
52	4.2.1	Full 2016 dataset and MC samples . . . . .	58
53	4.2.2	Triggers . . . . .	61
54	4.2.2.1	Trigger efficiency scale factors . . . . .	61
55	4.3	Object Identification and event selection . . . . .	62
56	4.3.1	Jets and $b$ tagging . . . . .	62
57	4.3.2	Lepton selection . . . . .	63
58	4.3.3	Lepton selection efficiency . . . . .	64
59	4.4	Background predictions . . . . .	65
60	4.5	Signal discrimination . . . . .	66
61	4.5.1	Classifiers response . . . . .	70
62	4.6	Additional discriminating variables . . . . .	73

63	<b>5 The CMS forward pixel detector</b>	<b>76</b>
64	5.0.1 The phase 1 FPix upgrade . . . . .	76
65	5.0.2 FPix module production line . . . . .	76
66	5.0.3 The Gluing stage . . . . .	76
67	5.0.4 The Encapsulation stage . . . . .	76
68	5.0.5 The FPix module production yields . . . . .	76
69	<b>Bibliography</b>	<b>76</b>
70	<b>References</b>	<b>77</b>

# <sup>71</sup> List of Figures

72	1.1	$^{14}N$ neutron capture in a PECVD polymerized pyridine film. The Q-value of this reaction is 626 keV. Taken from [22] . . . . .	1
74	2.1	Standard model of particle physics. . . . .	6
75	2.2	WI transformations between quarks . . . . .	13
76	2.3	Fundamental interactions in nature. . . . .	14
77	2.4	SM interactions diagrams . . . . .	15
78	2.5	Neutral current processes . . . . .	22
79	2.6	Spontaneous symmetry breaking mechanism . . . . .	29
80	2.7	SSB Potential form . . . . .	30
81	2.8	Potential for complex scalar field . . . . .	31
82	2.9	SSB mechanism for complex scalar field . . . . .	32
83	2.10	Proton-Proton collision . . . . .	39
84	2.11	Higgs production mechanism Feynman diagrams . . . . .	40
85	2.12	Higgs production cross section and decay branching ratios . . . . .	41
86	2.13	Associated Higgs production mechanism Feynman diagrams . . . . .	43
87	2.14	Cross section for $tHq$ process as a function of $C_t$ . . . . .	46
88	2.15	Cross section for $tHW$ process as a function of $\kappa_{Htt}$ . . . . .	46

89	3.1	ref. C.Lefevre, “The CERN accelerator complex,” (2008). CERN-DI-	
90		0812015. . . . .	51
91	3.2	ref. J.-L. Caron , “Layout of the LEP tunnel including future LHC in-	
92		frastructures.. L’ensemble du tunnel LEP avec les futures infrastructures	
93		LHC.”, <a href="https://cds.cern.ch/record/841542">https://cds.cern.ch/record/841542</a> (Nov, 1993). AC Collection.	
94		Legacy of AC. Pictures from 1992 to 2002.. . . . .	52
95	3.3	ref. ACTeam, “Diagram of an LHC dipole magnet. Schéma d’un aimant	
96		dipôle du LHC,” (1999). CERN-DI-9906025. . . . .	53
97	3.4	ref: CMS Collaboration, “Detector Drawings”, CMS-PHO-GEN-2012-002,	
98		<a href="http://cds.cern.ch/record/1433717">http://cds.cern.ch/record/1433717</a> , 2012. . . . .	55
99	4.1	The two leading-order diagrams of $tHq$ production. . . . .	57
100	4.2	Input variables to the BDT for signal discrimination normalized. . . . .	67
101	4.3	Input variables to the BDT for signal discrimination not normalized. . .	69
102	4.4	BDT inputs as seen by TMVA against $t\bar{t}$ . . . . .	70
103	4.5	BDT inputs as seen by TMVA against $t\bar{t}V$ . . . . .	71
104	4.6	Correlation matrices for the input variables in the TMVA. . . . .	72
105	4.7	MVA classifiers performance. . . . .	72
106	4.8	Additional discriminating variables distributions. . . . .	74

# <sup>107</sup> List of Tables

108	2.1	Fermions of the SM. . . . .	7
109	2.2	Leptons properties. . . . .	10
110	2.3	Quarks properties. . . . .	10
111	2.4	Fermion weak isospin and weak hypercharge multiplets. . . . .	12
112	2.5	Fundamental interactions features. . . . .	16
113	2.6	SM gauge bosons. . . . .	21
114	2.7	Higgs boson properties. . . . .	38
115	2.8	Predicted branching ratios for a SM Higgs boson with $m_H = 125 \text{ GeV}/c^2$ . . . . .	42
116	2.9	Predicted SM cross sections for $tH$ production at $\sqrt{s} = 13 \text{ TeV}$ . . . . .	44
117	2.10	Predicted enhancement of the $tHq$ and $tHW$ cross sections at LHC . . . . .	47
118	2.11	Predicted enhancement of the $tHq$ and $tHW$ cross sections at LHC . . . . .	48
119	4.1	Signal samples and their cross section and branching fraction. . . . .	58
120	4.2	$\kappa_V$ and $\kappa_t$ combinations. . . . .	59
121	4.3	List of background samples used in this analysis (CMSSW 80X). . . . .	60
122	4.4	Leading-order $t\bar{t}W$ and $t\bar{t}Z$ samples used in the signal BDT training. . . .	60
123	4.5	Table of high-level triggers that we consider in the analysis. . . . .	61
124	4.6	Trigger efficiency scale factors and associated uncertainties. . . . .	62
125	4.7	Requirements on each of the three muon selections. . . . .	63

126	4.8	Criteria for each of the three electron selections. . . . .	64
127	4.9	MVA input discriminating variables . . . . .	68
128	4.10	TMVA input variables ranking for BDTA_GRAD method . . . . .	73
129	4.11	TMVA configuration used in the BDT training. . . . .	73
130	4.12	ROC-integral for all the testing cases. . . . .	75

<sup>131</sup> Chapter 1

<sup>132</sup> INTRODUCTION

**Figure 1.1:**  $^{14}N$  neutron capture in a PECVD polymerized pyridine film. The Q-value of this reaction is 626 keV. Taken from [22]

# <sup>133</sup> Chapter 2

## <sup>134</sup> Theoretical approach

### <sup>135</sup> 2.1 Introduction

<sup>136</sup> The physical description of the universe is a challenge that physicists have faced by  
<sup>137</sup> making theories that refine existing principles and proposing new ones in an attempt  
<sup>138</sup> to embrace emerging facts and phenomena. By early 1800's, there were separate the-  
<sup>139</sup> ories describing electric and magnetic phenomena, gravitational force and light. The  
<sup>140</sup> invention of the electric battery by Alessandro Volta in 1800, the discovery of the  
<sup>141</sup> magnetic effects of the electric current by Oersted and Ampere (1820), and the gen-  
<sup>142</sup> eration of electric current using changing magnetic fields by Faraday (1831) represent  
<sup>143</sup> the first steps in the way to create a unified theory of electromagnetism [1].

<sup>144</sup>

<sup>145</sup> The unification was carried out by James Clerk Maxwell who was able to merge elec-  
<sup>146</sup> tricity and magnetism in a set of 20 equations known as "general equations of the  
<sup>147</sup> electromagnetic field," relating the observables that describe the experimental laws of  
<sup>148</sup> the electromagnetism. By combining these equations, Maxwell found a wave equation  
<sup>149</sup> and propose the existence of the "electromagnetic waves." The predicted propagation

150 speed of the electromagnetic waves turned out to be the same as the speed of light,  
151 therefore, the natural conclusion was that light is an electromagnetic wave [4]. By  
152 1900, waves were considered a perturbation of a material medium which in the case  
153 of the electromagnetic waves was identified as the “*Luminiferous Ether*”.

154

155 By 1900, Max Planck came out with the idea that radiation is quantized [5] and Albert  
156 Einstein in 1905 made use of that hypothesis to propose the existence of the light  
157 quantum, the “*photon*”, in order to explain the photoelectric effect [6]. The well-  
158 known quantum revolution in physics started and the idea of particle-wave duality  
159 of photons as a natural behavior was developed and later extended to electrons and  
160 to all kind of particles in nature. The development of a quantum theory allowed to  
161 predict a set of non-common sense effects like the quantum tunneling and quantum  
162 entanglement, however, quantum theory was separated from the recently unified elec-  
163 tromagnetism.

164

165 In 1905, Einstein also published two more papers; one aimed to describe his statistical  
166 molecular theory of liquids and how it can be used to describe Brownian motion [7].  
167 At that time the existence of the atoms and molecules were not fully demonstrated  
168 but Einstein’s theory provided an explanation as well as predictions based on the  
169 their existence. Jean Perrin in 1908 conducted experiments that confirmed Einstein’s  
170 predictions. The other paper described the relationship between space and time [8],  
171 unifying the notion of space and time into one entity known as “*spacetime*” that treats  
172 space and time at the same level and then discards the absoluteness of time. The  
173 new theory known as special relativity, supersedes the Galilean relativity principle  
174 and postulates exceptional effects like the time dilation, length contraction and mass-

175 energy equivalence through the most famous formula in physics [9]

$$E = mc^2. \quad (2.1)$$

176 Generalization of the special relativity was presented in 1916 and includes a gener-  
177 alization of Newton's law of universal gravitation, becoming a unified description of  
178 gravity as a geometric property of space and time. Einstein's predictions include the  
179 existence of black holes and the recently observed "*gravitational waves*" [10].

180 At the end of 1940s Julian Schwinger [11] and Richard P. Feynman [12], based in  
181 the work of Sin-Itiro Tomonaga [13], developed an electromagnetic theory consistent  
182 with special relativity and quantum mechanics that describes how matter and light  
183 interact; so-called "quantum eletrodynamics" (QED) had born.

184

185 QED has become the guide in the development of theories that describe the universe.  
186 It was the first example of a quantum field theory (QFT), which is the theoretical  
187 framework for building quantum mechanical models that describes particles and their  
188 interactions. QFT is composed of a set of mathematical tools that combines classical  
189 fields, special relativity, and quantum mechanics while keeping the quantum point  
190 particles and locality ideas. This chapter gives an overview of the SM, starting with  
191 the SM particle content, followed by a description of the electroweak interaction, the  
192 Higgs boson and the associated production of Higgs boson and a single top quark  
193 ( $tH$ ). The description contained in this chapter is based on references [1–3].

## 194 2.2 Standard model of particle physics

195 Particle physics at the fundamental level is modeled in terms of a collection of in-  
196 teracting particles and fields in a theory known as the “standard model of particle  
197 physics (SM)”<sup>1</sup>.

198 The full picture of the SM is composed of three fields<sup>2</sup>, whose excitations are inter-  
199 preted as particles called mediators or force-carriers; a set of fields, whose excitations  
200 are interpreted as elementary particles, interacting through the exchange of those  
201 mediators and a field that give the mass to elementary particles. Figure 2.1 shows an  
202 scheme of the SM particles organization. In addition to the particles in the scheme,  
203 their corresponding anti-particles, with opposite quantum numbers, are also part of  
204 the picture; some particles are their own anti-particles, like photon or Higgs, or anti-  
205 particle is already listed like in the  $W^+$  and  $W^-$  case.

206

207 The mathematical formulation of the SM is based on group theory and the use of  
208 Noether’s theorem [17] which states that for a physical system modeled by a La-  
209 grangian that is invariant under a group of transformations a conservation law is  
210 expected. For instance, a system described by a time-independent Lagrangian is  
211 invariant (symmetric) under time changes (transformations) with the total energy  
212 conservation law as the expected conservation law. In QED, the  $Q$  operator is the  
213 generator of the  $U(1)$  symmetry which according to the Noether’s theorem means  
214 that there is a conserved charge; this conserved charge is the electric charge and thus  
215 the law conservation of electric charge is established.

---

<sup>1</sup> The formal and complete treatment of the SM is out of the scope of this document, however a plenty of textbooks describing it at several levels are available in the literature. The treatment in “An Introduction To Quantum Field Theory (Frontiers in Physics)” by Michael E. Peskin and Dan V. Schroeder is quite comprehensive and detailed.

<sup>2</sup> Note that gravitational field is not included in the standard model formulation

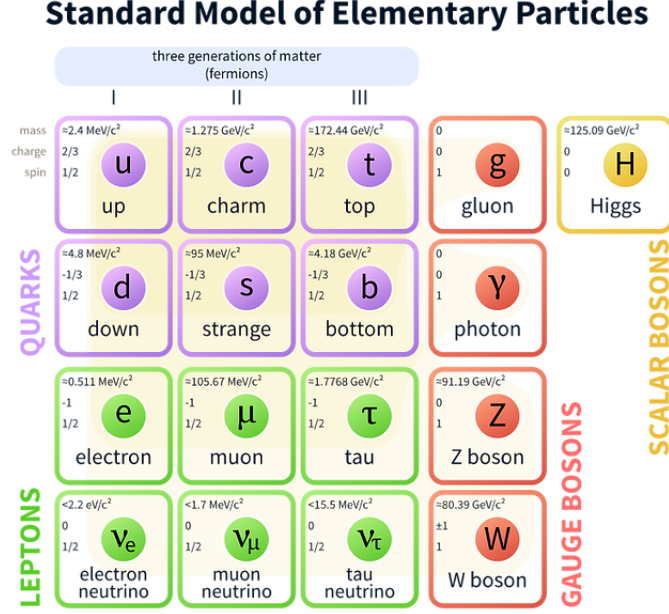


**Figure 2.1:** Schematic representation of the Standard model of particle physics. SM is a theoretical model intended to describe three of the four fundamental forces of the universe in terms of a set of particles and their interactions. [18].

216

217 In the SM, the symmetry group  $SU(3)_C \otimes SU(2)_L \otimes U(1)_Y$  describes three of the  
 218 four fundamental interactions in nature(see section 2.2.2): strong interaction(SI),  
 219 weak interaction(WI) and electromagnetic interactions (EI) in terms of symmetries  
 220 associated to physical quantities:

- 221     • Strong:  $SU(3)_C$  associated to color charge  
 222     • Weak:  $SU(2)_L$  associated to weak isospin and chirality  
 223     • Electromagnetic:  $U(1)_Y$  associated to weak hypercharge and electric charge

224 It will be shown that the electromagnetic and weak interactions are combined in  
 225 the so-called electroweak interaction where chirality, hypercharge, weak isospin and  
 226 electric charge are the central concepts.

## 227 2.2.1 Fermions

228 The basic constituents of the ordinary matter at the lowest level, which form the set  
 229 of elementary particles in the SM formulation, are quarks and leptons. All of them  
 230 have spin 1/2, therefore they are classified as fermions since they obey Fermi-Dirac  
 231 statistics. In both cases, they come in six “flavors” and are organized in three gener-  
 232 ations, or families, as shown in table 2.1.

233

234 There is a mass hierarchy between generations where the higher generation particles  
 235 decays to the lower one which can explain why the ordinary matter is made of particles  
 236 in the first generation. In the SM, neutrinos are modeled as massless particles so they  
 237 are not subject to this mass hierarchy; however, today it is known that neutrinos are  
 238 massive so the hierarchy could be restated. The reason behind this mass hierarchy is  
 239 one of the most important open questions in particle physics, and it becomes more  
 240 puzzling when noticing that the mass difference between first and second generation  
 241 fermions is small compared to the mass difference with respect to the third generation.  
 242 Usually, the second and third generation fermions are produced in high energy pro-  
 243 cesses, like the ones recreated in the particle accelerators.

		Generation		
		1st	2nd	3rd
Leptons	Type	Electron (e)	Moun( $\mu$ )	Tau ( $\tau$ )
	Charged Neutral	Electron neutrino ( $\nu_e$ )	Muon neutrino ( $\nu_\mu$ )	Tau neutrino ( $\nu_\tau$ )
Quarks	Up-type Down-type	Up (u) Down (d)	Charm (c) Starnge (s)	Top (t) Bottom (b)

**Table 2.1:** Fermions of the SM. Quarks and leptons comes in six flavors each and are organized in three generations or families composed of two pairs of closely related particles. The close relationship is motivated by the fact that WI between leptons is limited to the members of the same generation. Generations differs by mass in a way that have been interpreted as a masss hierarchy.

244

245 **2.2.1.1 Leptons**

246 A lepton is an elementary particle that is not subject to the SI. As seen in table 2.1,  
 247 there are two types of leptons, the charged ones (electron, muon and tau) and the  
 248 neutral ones (the three neutrinos). The electric charge ( $Q$ ) is the property that gives  
 249 leptons the ability to participate in the EI. From the classical point of view,  $Q$  plays  
 250 a central role determining, among others, the strength of the electric field through  
 251 which the electromagnetic force is exerted. It is clear that neutrinos are not affected  
 252 by EI because they don't carry electric charge.

253

254 Another feature of the leptons that is fundamental in the mathematical description  
 255 of the SM is the chirality, which is closely related to spin and helicity. Helicity de-  
 256 fine the handedness of a particle by relating its spin and momentum such that if  
 257 they are parallel then the particle is right-handed; if spin and momentum are an-  
 258 tiparallel the particle is said to be left-handed. The study of parity conservation  
 259 (or violation) in  $\beta$ -decay have shown that only left-handed electrons/neutrinos or  
 260 right-handed positrons/anti-neutrinos are created [19]; the inclusion of that feature  
 261 in the theory was reached by using projection operators for helicity, however, helicity  
 262 is frame dependent for massive particles which makes it not Lorentz invariant and  
 263 then another related attribute has to be used: *chirality*.

264

265 Chirality is a purely quantum attribute which makes it not so easy to describe in  
 266 graphical terms but it defines how the wave function of a particle transforms under  
 267 certain rotations. As with helicity, there are two chiral states, left-handed chiral  
 268 (L) and right-handed chiral (R). In the highly relativistic limit where  $E \approx p \gg m$   
 269 helicity and chirality converge, becoming exactly the same for massless particles. In

270 the following when referring to left-handed (right-handed) it means left-handed chiral  
 271 (right-handed chiral). The fundamental fact about chirality is that while EI and SI  
 272 are not sensitive to chirality, in WI left-handed and right-handed fermions are treated  
 273 asymmetrically, such that only left handed fermions and right-handed anti-fermions  
 274 are allowed to couple to WI mediators, which is a violation of parity. The way to  
 275 translate this statement in a formal mathematical formulation is based on the isospin  
 276 symmetry group  $SU(2)_L$ .

277 Each generation of leptons is seen as a weak isospin doublet.<sup>3</sup> The left-handed charged  
 278 lepton and its associated left-handed neutrino are arranged in doublets of weak isospin  
 279 T=1/2 while their right-handed partners are singlets:

$$\begin{pmatrix} \nu_l \\ l_R \end{pmatrix}_L, l_R := \begin{pmatrix} \nu_e \\ e \end{pmatrix}_L, \begin{pmatrix} \nu_\mu \\ \mu \end{pmatrix}_L, \begin{pmatrix} \nu_\tau \\ \tau \end{pmatrix}_L, e_R, \mu_R, \tau_R, \nu_{eR}, \nu_{\mu R}, \nu_{\tau R} \quad (2.2)$$

280 The isospin third component refers to the eigenvalues of the weak isospin operator  
 281 which for doublets is  $T_3 = \pm 1/2$ , while for singlets it is  $T_3 = 0$ . The physical meaning  
 282 of this doublet-singlet arrangement falls in that the WI couples the two particles in  
 283 the doublet by exchanging the interaction mediator while the singlet member is not  
 284 involved in WI. The main properties of the leptons are summarized in table 2.2.

285

286 Altough all three flavor neutrinos have been observed, their masses remain unknown  
 287 and only some estimations have been made [20]. The main reason is that the fla-  
 288 vor eigenstates are not the same as the mass eigenstates which imply that when a  
 289 neutrino is created its mass state is a linear combination of the three mass eigen-  
 290 states and experiments can only probe the squared difference of the masses. The  
 291 Pontecorvo-Maki-Nakagawa-Sakata (PMNS) mixing matrix encode the relationship

---

<sup>3</sup> The weak isospin is an analogy of the isospin symmetry in strong interaction where neutron and proton are affected equally by strong force but differ in their charge.

292 between flavor and mass eigenstates.

Lepton	Q(e)	$T_3$	$L_e$	$L_\mu$	$L_\tau$	Mass (MeV/c <sup>2</sup> )	Lifetime (s)
Electron (e)	-1	-1/2	1	0	0	0.5109989461(31)	Stable
Electron neutrino( $\nu_e$ )	0	1/2	1	0	0	Unknown	Unknown
Muon ( $\mu$ )	-1	-1/2	0	1	0	105.6583745(24)	$2.1969811(22) \times 10^{-6}$
Muon neutrino ( $\nu_\mu$ )	0	1/2	0	1	0	Unknown	Unknown
Tau ( $\tau$ )	-1	-1/2	0	0	1	1776.86(12)	$290.3(5) \times 10^{-15}$
Tau neutrino ( $\tau_\mu$ )	0	1/2	0	0	1	Unknown	Unknown

**Table 2.2:** Leptons properties [21]. Q: electric charge,  $T_3$ : weak isospin. Only left-handed leptons and right-handed anti-leptons participate in the WI. Anti-particles with inverted  $T_3$ , Q and lepton number complete the leptons set but are not listed. Right-handed leptons and left-handed anti-leptons, neither listed, form weak isospin singlets with  $T_3 = 0$  and do not take part in the weak interaction.

293

### 294 2.2.1.2 Quarks

295 Quarks are the basic constituents of protons, neutrons and other non-elementary  
 296 particles. The way quarks join to form bound states, called “hadrons”, is through the  
 297 SI. Quarks are affected by all the fundamental interactions which means that they  
 298 carry all the four types of charges: color, electric charge, weak isospin and mass.

Flavor	Q(e)	$I_3$	$T_3$	B	C	S	T	$B'$	Y	Color	Mass (MeV/c <sup>2</sup> )
Up (u)	2/3	1/2	1/2	1/3	0	0	0	0	1/3	r,b,g	$2.2^{+0.6}_{-0.4}$
Charm (c)	2/3	0	1/2	1/3	1	0	0	0	4/3	r,b,g	$1.28 \pm 0.03 \times 10^3$
Top(t)	2/3	0	1/2	1/3	0	0	1	0	4/3	r,b,g	$173.1 \pm 0.6 \times 10^3$
Down(d)	-1/3	-1/2	-1/2	1/3	0	0	0	0	1/3	r,b,g	$4.7^{+0.5}_{-0.4}$
Strange(s)	-1/3	0	-1/2	1/3	0	-1	0	0	-2/3	r,b,g	$96^{+8}_{-4}$
Bottom(b)	-1/3	0	-1/2	1/3	0	0	0	-1	-2/3	r,b,g	$4.18^{+0.04}_{-0.03} \times 10^3$

**Table 2.3:** Quarks properties [21]. Q: electric charge,  $I_3$ : isospin,  $T_3$ : weak isospin, B: baryon number, C: charmness, S: strangeness, T: topness,  $B'$ : bottomness, Y: hypercharge. Anti-quarks posses the same mass and spin as quarks but all charges (color, flavor numbers) have opposite sign.

299

300 Table 2.3 summarizes the features of quarks, among which the most particular is  
 301 their fractional electric charge. Note that fractional charge is not a problem, given  
 302 that quarks are not found isolated, but serves to explain how composed particles are  
 303 formed out of two or more valence quarks<sup>4</sup>.

304

305 Color charge is the responsible for the SI between quarks and is the symmetry  
 306 ( $SU(3)_C$ ) that defines the formalism to describe SI. There are three colors: red (r),  
 307 blue(b) and green(g) and their corresponding three anti-colors; thus each quark carries  
 308 one color unit while anti-quarks carries one anti-color unit. As said above, quarks are  
 309 not allowed to be isolated due to the color confinement effect, therefore their features  
 310 have been studied indirectly by observing their bound states created when:

311     • one quark with a color charge is attracted by an anti-quark with the correspond-  
 312         ing anti-color charge forming a colorless particle called a “meson.”

313     • three quarks (anti-quarks) with different color (anti-color) charges are attracted  
 314         among them forming a colorless particle called a “baryon(anti-baryon).”

315 In the first version of the quark model (1964), M. Gell-Mann [22] and G. Zweig [23,24]  
 316 developed a consistent way to classify hadrons according to their properties. Only  
 317 three quarks (u, d, s) were involved in a scheme in which all baryons have baryon  
 318 number  $B=1$  and therefore quarks have  $B=1/3$ ; non-baryons have  $B=0$ . The scheme  
 319 organize baryons in a two-dimensional space ( $I_3 - Y$ );  $Y$  (hypercharge) and  $I_3$  (isospin)  
 320 are quantum numbers related by the Gell-Mann-Nishijima formula [25, 26]:

$$Q = I_3 + \frac{Y}{2} \quad (2.3)$$

---

<sup>4</sup> Hadrons can contain an indefinite number of virtual quarks and gluons, known as the quark and gluon sea, but only the valence quarks determine hadrons' quantum numbers.

321 where  $Y = B + S + C + T + B'$  are the quantum numbers listed in table 2.3. Baryon  
 322 number is conserved in SI and EI which means that single quarks cannot be created  
 323 but in pairs  $q - \bar{q}$ .

324

325 Similar to leptons, there are six quark flavors organized in three generations (see table  
 326 2.1) and follow a mass hierarchy which again implies that higher generations decay  
 327 to first generation quarks.

	Quarks			$T_3$	$Y_W$	Leptons			$T_3$	$Y_W$
Doublets	$(\begin{smallmatrix} u \\ d' \end{smallmatrix})_L$	$(\begin{smallmatrix} c \\ s' \end{smallmatrix})_L$	$(\begin{smallmatrix} t \\ b' \end{smallmatrix})_L$	$(\begin{smallmatrix} 1/2 \\ -1/2 \end{smallmatrix})$	1/3	$(\begin{smallmatrix} \nu_e \\ e \end{smallmatrix})_L$	$(\begin{smallmatrix} \nu_\mu \\ \mu \end{smallmatrix})_L$	$(\begin{smallmatrix} \nu_\tau \\ \tau \end{smallmatrix})_L$	$(\begin{smallmatrix} 1/2 \\ -1/2 \end{smallmatrix})$	-1
Singlets	$u_R$	$c_R$	$t_R$	0	4/3	$\nu_{eR}$	$\nu_{\mu R}$	$\nu_{\tau R}$	0	-2
	$d'_R$	$s'_R$	$b'_R$	0	-2/3	$e_R$	$\mu_R$	$\tau_R$	0	-2

**Table 2.4:** Fermion weak isospin and weak hypercharge multiplets. Weak hypercharge is calculated through the Gell-Mann-Nishijima formula 2.3 but using the weak isospin and charge for quarks.

328

329 Isospin doublets of quarks are also defined (see table 2.4) and as for neutrinos, the  
 330 mass eigenstates are not the same as the WI eigenstates which means that members of  
 331 different quark generations are connected by the WI mediator; thus, up-type quarks  
 332 are coupled not to down-type quarks directly but to a superposition of down-type  
 333 quarks ( $q'_d$ ) via WI according to:

$$334 \quad q'_d = V_{CKM} q_d$$

$$\begin{pmatrix} d' \\ s' \\ b' \end{pmatrix} = \begin{pmatrix} V_{ud} & V_{us} & V_{ub} \\ V_{cd} & V_{cs} & V_{cb} \\ V_{td} & V_{ts} & V_{tb} \end{pmatrix} \begin{pmatrix} d \\ s \\ b \end{pmatrix} \quad (2.4)$$

335 where  $V_{CKM}$  is known as Cabibbo-Kobayashi-Maskawa (CKM) mixing matrix [27,28].

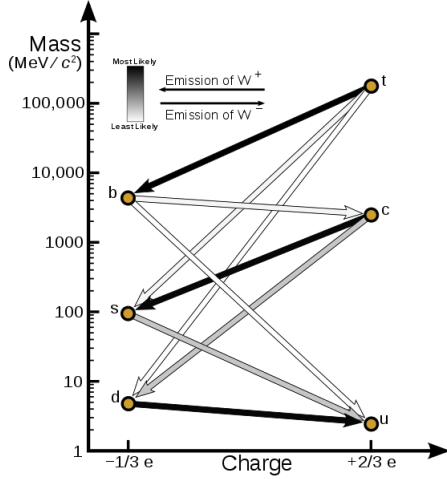


**Figure 2.2:** Transformations between quarks through WI. Higher generations quarks decay to first generation quarks by emitting a W boson. The arrow color indicates the likelihood of the transition according to the grey scale in the top left side which represent the CKM matrix parameters [29].

336 The weak decays of quarks are represented in the diagram of figure 2.2; again the  
 337 CKM matrix plays a central role since it contains the probabilities for the different  
 338 quark decay channels, in particular, note that quark decays are greatly favored be-  
 339 tween generation members.

340

341 CKM matrix is a  $3 \times 3$  unitary matrix parametrized by three mixing angles and the  
 342 *CP-mixing phase*; the latter is the parameter responsible for the CP-violation in the  
 343 SM. The fact that the b quark decays almost all the times to a top quark is exploited  
 344 in this thesis when making the selection of the signal events by requiring the presence  
 345 of a jet tagged as a jet coming from a b quark in the final state. The effect of the  
 346 *CP-mixing phase* on the cross section of associated production of Higgs boson and a  
 347 single top process is also explored in this thesis.

## Fundamental interactions.

Illustration: Typoform

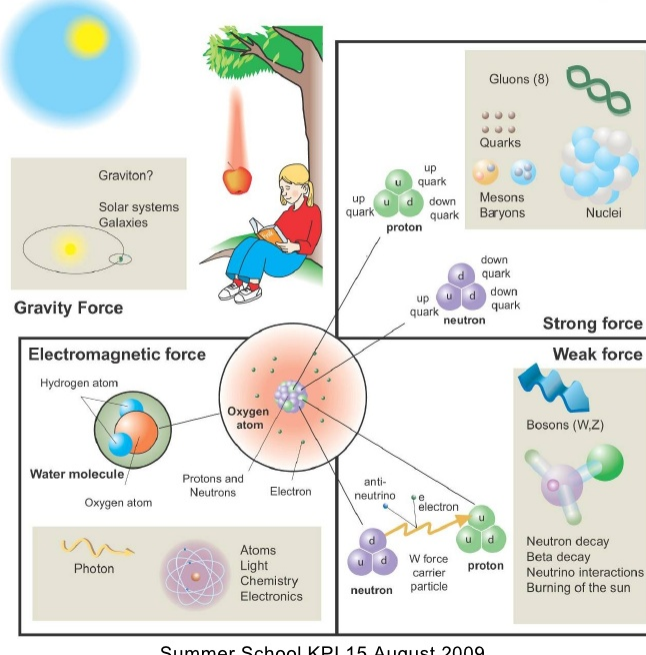


**Figure 2.3:** Fundamental interactions in nature. Despite the many manifestations of forces in nature, we can track all of them back to one of the fundamental interactions. The most common forces are gravity and electromagnetic given that all of us are subject and experience them in everyday life.

### 348 2.2.2 Fundamental interactions

349 Even though there are many manifestations of force in nature, like the ones represented in figure 2.3, we can classify all of them into one of four fundamental interactions:

352 • *Electromagnetic interaction (EI)* affect particles that are “electrically charged,”  
 353 like electrons and protons. It is described by QED combining quantum mechanics,  
 354 special relativity and electromagnetism in order to explain how particles  
 355 with electric charge interact through the exchange of photons, therefore, one  
 356 says that “Electromagnetic Force” is mediated by “photons”. Figure 2.4a) shows  
 357 a graphical representation, known as “feynman diagram”, of electron-electron

358 scattering.

359 • *Strong interaction (SI)* described by Quantum Chromodynamics (QCD). Hadrons  
 360 like proton and neutron have internal structure given that they are composed  
 361 of two or more valence quarks<sup>5</sup>. Quarks have fractional electric charge which  
 362 means that they are subject to electromagnetic interaction and in the case of the  
 363 proton they should break apart due to electrostatic repulsion; however, quarks  
 364 are held together inside the hadrons against their electrostatic repulsion by the  
 365 “Strong Force” through the exchange of “gluons.” The analog to the electric  
 366 charge is the “color charge”. Electrons and photons are elementary particles  
 367 as quarks but they don’t carry color charge, therefore they are not subject to  
 368 SI. The feynman diagram for gluon exchange between quarks is shown in figure  
 369 2.4b).

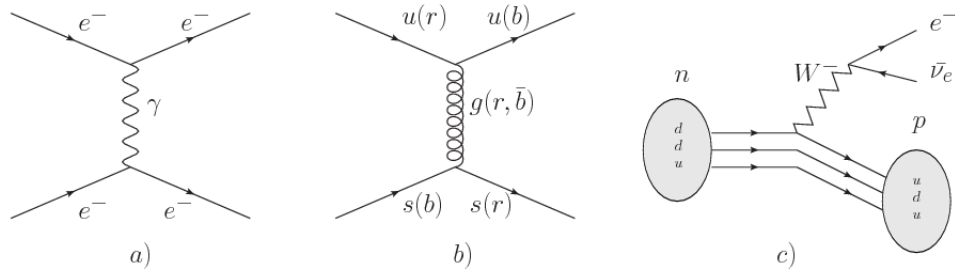


**Figure 2.4:** Feynman diagrams representing the interactions in SM; a) EI:  $e$ - $e$  scattering; b) SI: gluon exchange between quarks ; c) WI:  $\beta$ -decay

370 • *Weak interaction (WI)* described by the Weak theory (WT), is responsible for  
 371 instance for the radioactive decay in atoms and proton-proton (pp) fusion within  
 372 the sun. Quarks and leptons are the particles affected by the weak interaction  
 373 and posses a property called “flavor charge” which can be changed by emitting  
 374 or absorbing one weak force mediator; they comes in six flavors each (see 2.2.1).  
 375 There are three mediators of the “Weak force” known as “Z” boson in the case of

<sup>5</sup> particles made of four and five quarks are exotic states not so common

376 electrically neutral changes and “ $W^\pm$ ” bosons in the case of electrically charged  
 377 changes. The “weak isospin” is the WI analog to electric charge in EI and color  
 378 charge in SI and define how quarks and leptons are affected by the weak force.  
 379 Figure 2.4c) shows the feynman diagram of  $\beta$ -decay where a newtron (n) is  
 380 transformed in a proton (p) by emmiting a  $W^-$  particle. Since this thesis is in  
 381 the frame of the electroweak interaction, a more detailed description of it will  
 382 be given in section 2.3

383 • *Gravitational interaction (GI)* described by General Theory of Relativity (GR).  
 384 It is responsible for the structure of galaxies and black holes as well as the  
 385 expansion of the universe. As a classical theory, in the sense that it can be  
 386 formulated without even appeal to the concept of quantization, it implies that  
 387 the spacetime is a continuum and predictions can be made without limitation  
 388 to the precision of the measurement tools which represent a direct contradiction  
 389 of the quantum mechanics principles. Gravity is deterministic while quantum  
 390 mechanics is probabilistic; despite that, efforts to develop a quantum theory of  
 391 gravity have predicted the “graviton” as mediator of the Gravitational force<sup>6</sup>.

Interaction	Acts on	Relative strength	Range (m)	Mediators
Electromagnetic (QED)	Electrically charged particles	$10^{-2}$	Infinite	Photon
Strong (QCD)	Quarks and gluons	1	$10^{-15}$	Gluon
Weak (WI)	Leptons and quarks	$10^{-6}$	$10^{-18}$	$W^\pm$ , Z
Gravitational (GI)	Massive particles	$10^{-39}$	Infinite	Graviton

**Table 2.5:** Fundamental interactions features [30].

392

393 Table 2.5 summarizes the main features of the fundamental interactions. The rela-  
 394 tive strength of the fundamental forces reveals the meaning of strong and weak;

<sup>6</sup> Actually a wide variety of theories have been developed in an attempt to describe gravity; some famous examples are string theory and supergravity.

395 a context where the relative strength of the SI is 1, the EI is about hundred times  
 396 weaker and WI is about million times weaker than the SI. A good description on  
 397 how the relative strength and range of the fundamental interactions are calculated  
 398 can be found in references [30, 31]. In the everyday life, only EI and GI are explicitly  
 399 experienced due to the range of these interactions; i.e., at the human scale distances  
 400 only EI and GI have appreciable effects, in contrast to SI which at distances greater  
 401 than  $10^{-15}$ m become negligible.

402

403 QED was built successfully on the basis of the classical electrodynamics theory of  
 404 Maxwell and Lorentz (CED), following theoretical and experimental requirements  
 405 imposed by

- 406     • lorentz invariance: independence on the reference frame.
- 407     • locallity: interacting fields are evaluated at the same space-time point to avoid  
     408       action at a distance.
- 409     • renormalizability: physical predictions are finite and well defined
- 410     • particle spectrum, symmetries and conservation laws already known must emerge  
     411       from the theory.
- 412     • gauge invariance.

413 The gauge invariance requirement reflects the fact that the fundamental fields cannot  
 414 be directly measured but associated fields which are the observables. Electric (“**E**”)  
 415 and magnetic (“**B**”) fields in CED are associated with the electric scalar potential  
 416 “**V**” and the vector potential “**A**”. In particular, **E** can be obtained by measuring  
 417 the change in the space of the scalar potential ( $\Delta V$ ); however, two scalar potentials

418 differing by a constant “f” correspond to the same electric field. The same happens  
 419 in the case of the vector potential “ $\mathbf{A}$ ”; thus, different configurations of the associated  
 420 fields result in the same set of values of the observables. The freedom in choosing  
 421 one particular configuration is known as “gauge freedom”; the transformation law  
 422 connecting two configurations is known as “gauge transformation” and the fact that  
 423 the observables are not affected by a gauge transformation is called “gauge invariance”.  
 424 When the gauge transformation:

$$\begin{aligned}\mathbf{A} &\rightarrow \mathbf{A} - \nabla f \\ V &\rightarrow V - \frac{\partial f}{\partial t}\end{aligned}\tag{2.5}$$

425 is applied to Maxwell equations, they are still satisfied and the fields remain invariant.  
 426 Thus, the classical electrodynamics theory is invariant under gauge transformations  
 427 and is called a “gauge theory”. The set of all gauge transformations form the “sym-  
 428 metry group” of the theory, which according to the group theory, has a set of “group  
 429 generators”. The number of group generators determine the number of “gauge fields”  
 430 of the theory.

431  
 432 As mentioned in the first lines of section 2.2, QED has one symmetry group ( $U(1)$ )  
 433 with one group generator (the  $Q$  operator) and one gauge field (the electromagnetic  
 434 field  $A^\mu$ ). In CED there is not a clear definition, beyond the historical convention, of  
 435 which fields are the fundamental and which are the associated, but in QED it is clear  
 436 that the fundamental field is  $A^\mu$ . When a gauge theory is quantized, the gauge field  
 437 is quantized and its quanta is called “gauge boson”. The word boson characterize  
 438 particles with integer spin which obey Bose-Einstein statistics.

439

440 As will be detailed in section 2.3, interactions between particles in a system can be  
 441 obtained by considering first the Lagrangian density of free particles in the system,  
 442 which of course is incomplete because the interaction terms have been left out, and  
 443 demanding global phase transformation invariance. Global phase transformation in-  
 444 variance means that a gauge transformation is performed identically to every point  
 445 in the space<sup>7</sup> and the Lagrangian remains invariant. Then, the global transformation  
 446 is promoted to a local phase transformation (this time the gauge transformation de-  
 447 pends on the position in space) and again invariance is required.

448

449 Due to the space dependence of the local transformation, the Lagrangian density is  
 450 not invariant anymore. In order to restate the gauge invariance, the gauge covariant  
 451 derivative is introduced in the Lagrangian and with it the gauge field responsible for  
 452 the interaction between particles in the system. The new Lagrangian density is gauge  
 453 invariant, includes the interaction terms needed to account for the interactions and  
 454 provide a way to explain the interaction between particles through the exchange of  
 455 the gauge boson.

456 This recipe was used to build QED and the theories that aim to explain the funda-  
 457 mental interactions.

### 458 **2.2.3 Gauge Bosons**

459 The importance of the gauge bosons comes from the fact that they are the force  
 460 mediators or force carriers. The features of the gauge bosons reflect the features of  
 461 the fields they represent; these features are extracted from the Lagrangian density used  
 462 to describe the interactions. In section 2.3, it will be shown how the gauge bosons

---

<sup>7</sup> Here space corresponds to the 4-dimensional space i.e. space-time.

463 of the EI and WI emerge from the electroweak Lagrangian. The SI gauge bosons  
 464 features are also extracted from the SI Lagrangian but it is not detailed in this  
 465 document. Here, the main features of the SM gauge bosons will be briefly presented  
 466 and summarized in table 2.6.

467     • **Photon.** EI occurs when the photon couples to (is exchanged between) particles  
 468 carrying electric charge; however, the photon itself does not carry electric charge,  
 469 therefore, there is no coupling between photons. Given that the photon is  
 470 massless the EI is of infinite range i.e. electrically charged particles interact  
 471 even if they are located far away one from each other; that also means that  
 472 photons always move with the speed of light.

473     • **Gluon.** SI is mediated by gluons, which same as photons are massless. They  
 474 carry one unit of color charge and one unit of anticolor charge which means that  
 475 gluons couples to other gluons. As a result, the range of the SI is not infinite  
 476 but very short due to the attraction between gluons, giving rise to the “color  
 477 confinement” which explains why color charged particles cannot be isolated but  
 478 live within composited particles, like quarks inside protons.

479     • **W, Z.** The EWI mediators,  $W^\pm$  and Z, are massive which explain its short-  
 480 range. Given that the WI is the only interaction that can change the flavor  
 481 of the interacting particles, the W boson is the responsible for the nuclear  
 482 transmutation where a neutron is converted in a proton or vice versa with the  
 483 involvement of an electron and a neutrino. The Z boson is the responsible of the  
 484 neutral weak processes like neutrino elastic scattering where no electric charge  
 485 but momentum transference is involved. WI gauge bosons carry isospin charge  
 486 which makes possible the interaction between them.

Interaction	Mediator	Electric charge (e)	Color charge	Weak Isospin	mass (GeV/c <sup>2</sup> )
Electromagnetic	Photon ( $\gamma$ )	0	No	0	0
Strong	Gluon (g)	0	Yes -octet	No	0
Weak	$W^\pm$ Z	$\pm 1$ 0	No No	$\pm 1$ 0	$80.385 \pm 0.015$ $91.188 \pm 0.002$

**Table 2.6:** SM gauge bosons main features [21].

487

## 488 2.3 Electroweak unification and the Higgs

### 489 mechanism

490 Physicist dreams of building a theory that contains all the interactions in one single  
 491 interaction, i.e. showing that at some scale in energy all the four fundamental in-  
 492 teractions are unified and only one interaction emerges in a “Theory of everything”.  
 493 The first sign of the feasibility of such unification comes from success in the con-  
 494 struction of the CED. Einstein spent years trying to reach that dream, which by  
 495 1920 only involved electromagnetism and gravity, with no success; however, a new  
 496 partial unification was achieved in the 1960’s, when S.Glashow [14], A.Salam [15] and  
 497 S.Weinberg [16] independently proposed that electromagnetic and weak interactions  
 498 are two manifestations of a more general interaction called “electroweak interaction.”  
 499 QCD and EWT were developed in parallel and following the useful prescription pro-  
 500 vided by QED and the gauge invariance principles.

501

502 The theory of weak interactions was capable of explaining the  $\beta$ -decay and in general  
 503 the processes mediated by  $W^\pm$  bosons. However, there were some processes like the  
 504 “ $\nu_\mu - e$  scattering” which would require the exchange of two W bosons (see figure 2.5  
 505 top diagrams) giving rise to divergent loop integrals and then non finite predictions.

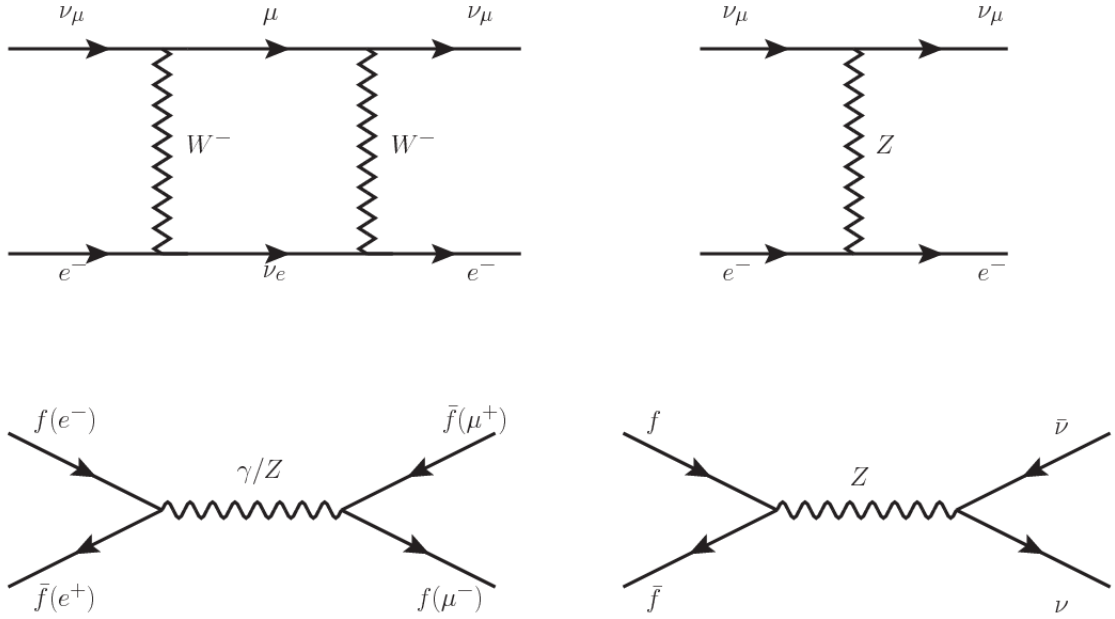


**Figure 2.5:** Top:  $\nu_\mu - e^-$  scattering going through charged currents (left) and neutral currents (right). Bottom: neutral current processes for charged fermions (left) and involving neutrinos (right). While neutral current processes involving only charged fermions can proceed through EI or WI, those involving neutrinos can only proceed via WI.

506 By including neutral currents involving fermions via the exchange of neutral bosons  
 507  $Z$ , those divergences are compensated and the predictions become realistic.  
 508 Neutral weak interaction vertices conserve flavor in the same way as the electromag-  
 509 netic vertices do, but additionally, the  $Z$  boson can couple to neutrinos which implies  
 510 that processes involving charged fermions can proceed through EI or WI but processes  
 511 involving neutrinos can proceed only through WI.

512

513 The prescription to build a gauge theory of the WI consist of proposing a free field La-  
 514 grangian density that includes the particles involved; next, by requesting invariance  
 515 under global phase transformations first and generalizing to local phase transfor-  
 516 mations invariance later, the conserved currents are identified and interactions are  
 517 generated by introducing gauge fields. Given that the goal is to include the EI and

518 WI in a single theory, the group symmetry considered should be a combination of  
 519  $SU(2)_L$  and  $U(1)_{em}$ , however the latter cannot be used directly because the EI treat  
 520 left and right-handed particles indistinctly in contrast to the former. Fortunately, the  
 521 weak hypercharge, which is a combination of the weak isospin and the electric charge  
 522 (eqn 2.3) is suitable to be used since it is conserved by the EI and WI. Thus, the  
 523 symmetry group to be considered is

$$G \equiv SU(2)_L \otimes U(1)_Y \quad (2.6)$$

524 The following treatment applies to any of the fermion generations but for simplicity  
 525 the first generation of leptons will be considered [2, 3, 32, 33]. Also, the unified weak  
 526 and electromagnetic interaction will be referred as “Electroweak Interaction (EWI).”  
 527 Given the first generation of leptons

$$\psi_1 = \begin{pmatrix} \nu_e \\ e^- \end{pmatrix}_L, \quad \psi_2 = \nu_{eR}, \quad \psi_3 = e_R^- \quad (2.7)$$

528 the charged fermionic currents are given by

$$J_\mu \equiv J_\mu^+ = \bar{\nu}_{eL} \gamma_\mu e_L, \quad J_\mu^\dagger \equiv J_\mu^- = \bar{e}_L \gamma_\mu \nu_{eL} \quad (2.8)$$

529 and the free Lagrangian is given by

$$\mathcal{L}_0 = \sum_{j=1}^3 i\bar{\psi}_j(x) \gamma^\mu \partial_\mu \psi_j(x). \quad (2.9)$$

530 Mass terms are included directly in the QED and QCD free Lagrangians since they  
 531 preserve the invariance under the symmetry transformations involved which treat  
 532 left-handed and right-handed similarly, however mass terms of the form

$$m_W^2 W_\mu^\dagger(x) W^\mu(x) + \frac{1}{2} m_Z^2 Z_\mu(x) Z^\mu(x) - m_e \bar{\psi}_e(x) \psi_e(x) \quad (2.10)$$

533 which represent the mass of  $W^\pm$ , Z and electrons, are not invariant under G trans-  
 534 formations, therefore the gauge fields described by the EWI are in principle massless.

535

536 Experiments have shown that the gauge fields are not massless; however, they have  
 537 to acquire mass through a mechanism compatible with the gauge invariance; that  
 538 mechanism is known as the “Higgs mechanism” and will be considered later in this  
 539 section. The global transformations in the combined symmetry group G can be  
 540 written as

$$\begin{aligned} \psi_1(x) &\xrightarrow{G} \psi'_1(x) \equiv U_Y U_L \psi_1(x), \\ \psi_2(x) &\xrightarrow{G} \psi'_2(x) \equiv U_Y \psi_2(x), \\ \psi_3(x) &\xrightarrow{G} \psi'_3(x) \equiv U_Y \psi_3(x) \end{aligned} \quad (2.11)$$

541 where  $U_L$  represent the  $SU(2)_L$  transformation acting on the weak isospin doublet  
 542 only and  $U_Y$  represent the  $U(1)_Y$  transformation acting on all the weak isospin mul-  
 543 tiplets. Explicitly

$$U_L \equiv \exp\left(i \frac{\sigma_i}{2} \alpha^i\right), \quad U_Y \equiv \exp(i y_i \beta) \quad (i = 1, 2, 3) \quad (2.12)$$

544 with  $\sigma_i$  the Pauli matrices and  $y_i$  the weak hypercharges. In order to promote the  
 545 transformations from global to local while keeping the invariance, it is required that  
 546  $\alpha^i = \alpha^i(x)$ ,  $\beta = \beta(x)$  and the replacement of the ordinary derivatives by the covariant  
 547 derivatives

$$\begin{aligned}
D_\mu \psi_1(x) &\equiv \left[ \partial_\mu + ig\sigma_i W_\mu^i(x)/2 + ig'y_1 B_\mu(x) \right] \psi_1(x) \\
D_\mu \psi_2(x) &\equiv \left[ \partial_\mu + ig'y_2 B_\mu(x) \right] \psi_2(x) \\
D_\mu \psi_3(x) &\equiv \left[ \partial_\mu + ig'y_3 B_\mu(x) \right] \psi_3(x)
\end{aligned} \tag{2.13}$$

548 introducing in this way four gauge fields,  $W_\mu^i(x)$  and  $B_\mu(x)$ , in the process. The  
549 covariant derivatives (eqn 2.13) are required to transform in the same way as fermion  
550 fields  $\psi_i(x)$  themselves, therefore, the gauge fields transform as:

$$\begin{aligned}
B_\mu(x) &\xrightarrow{G} B'_\mu(x) \equiv B_\mu(x) - \frac{1}{g'} \partial_\mu \beta(x) \\
W_\mu^i(x) &\xrightarrow{G} W_\mu^{i'}(x) \equiv W_\mu^i(x) - \frac{i}{g} \partial_\mu \alpha_i(x) - \varepsilon_{ijk} \alpha_i(x) W_\mu^j(x).
\end{aligned} \tag{2.14}$$

551 The G invariant version of the Lagrangian density 2.9 can be written as

$$\mathcal{L}_0 = \sum_{j=1}^3 i\bar{\psi}_j(x) \gamma^\mu D_\mu \psi_j(x) \tag{2.15}$$

552 where free massless fermion and gauge fields and fermion-gauge boson interactions  
553 are included. The EWI Lagrangian density must additionally include kinetic terms  
554 for the gauge fields ( $\mathcal{L}_G$ ) which are built from the field strengths, according to

$$B_{\mu\nu}(x) \equiv \partial_\mu B_\nu - \partial_\nu B_\mu \tag{2.16}$$

$$W_{\mu\nu}^i(x) \equiv \partial_\mu W_\nu^i(x) - \partial_\nu W_\mu^i(x) - g\varepsilon^{ijk} W_\mu^j W_\nu^k \tag{2.17}$$

555 the last term in eqn. 2.17 is added in order to hold the gauge invariance; therefore,

$$\mathcal{L}_G = -\frac{1}{4}B_{\mu\nu}(x)B^{\mu\nu}(x) - \frac{1}{4}W_{\mu\nu}^i(x)W_i^{\mu\nu}(x) \quad (2.18)$$

556 which contains not only the free gauge fields contributions but also the gauge fields  
 557 self-interactions and interactions among them.

558 The three weak isospin conserved currents resulting from the  $SU(2)_L$  symmetry are  
 559 given by

$$J_\mu^i(x) = \frac{1}{2}\bar{\psi}_1(x)\gamma_\mu\sigma^i\psi_1(x) \quad (2.19)$$

560 while the weak hypercharge conserved current resulting from the  $U(1)_Y$  symmetry is  
 561 given by

$$J_\mu^Y = \sum_{j=1}^3 \bar{\psi}_j(x)\gamma_\mu y_j\psi_j(x) \quad (2.20)$$

562 In order to evaluate the electroweak interactions modeled by an isovector fields  $W_\mu^i$   
 563 which couples to isospin currents  $J_\mu^i$  with strength  $g$  and additionally the singlet  
 564 field  $B_\mu$  which couples to the weak hypercharge current  $J_\mu^Y$  with strength  $g'/2$ , the  
 565 interaction Lagrangian density to be considered is

$$\mathcal{L}_I = -g J^{i\mu}(x) W_\mu^i(x) - \frac{g'}{2} J^Y{}^\mu(x) B_\mu(x) \quad (2.21)$$

566 Note that the weak isospin currents are not the same as the charged fermionic currents  
 567 that were used to describe the WI (eqn 2.8), since the weak isospin eigenstates are  
 568 not the same as the mass eigenstates, but they are closely related

$$J_\mu = \frac{1}{2}(J_\mu^1 + iJ_\mu^2), \quad J_\mu^\dagger = \frac{1}{2}(J_\mu^1 - iJ_\mu^2). \quad (2.22)$$

569 The same happen with the gauge fields  $W_\mu^i$  which are related to the mass eigenstates  
 570  $W^\pm$  by

$$W_\mu^+ = \frac{1}{\sqrt{2}}(W_\mu^1 - iW_\mu^2), \quad W_\mu^- = \frac{1}{\sqrt{2}}(W_\mu^1 + iW_\mu^2). \quad (2.23)$$

571 The fact that there are three weak isospin conserved currents is an indication that in  
 572 addition to the charged fermionic currents which couple charged to neutral leptons  
 573 there should be a neutral fermionic current that couples neutral fermions or electri-  
 574 cally charged fermions that has the same electric charge and thus does not imply  
 575 electric charge change. The third weak isospin current contains a term that is simi-  
 576 lar to the electromagnetic current ( $j_\mu^{em}$ ), indicating that there is a relation between  
 577 them and resembling the Gell-Mann-Nishijima formula 2.3 adapted to electroweak  
 578 interactions

$$Q = T_3 + \frac{Y_W}{2}. \quad (2.24)$$

579 Just as Q generates the  $U(1)_{em}$  symmetry, the weak hypercharge generates the  $U(1)_Y$   
 580 symmetry as said before. It is possible to write the relationship in terms of the currents  
 581 as

$$j_\mu^{em} = J_\mu^3 + \frac{1}{2}J_\mu^Y. \quad (2.25)$$

582 The neutral gauge fields  $W_\mu^3$  and  $B_\mu$  cannot be directly identified with the  $Z$  and the  
 583 photon fields since the photon interacts similarly with left and right-handed fermions;  
 584 however, they are related through a linear combination given by

$$A_\mu = B_\mu \cos \theta_W + W_\mu^3 \sin \theta_W \quad (2.26)$$

$$Z_\mu = -B_\mu \sin \theta_W + W_\mu^3 \cos \theta_W$$

585 where  $\theta_W$  is known as the “Weinberg angle.” The interaction Lagrangian is now given

586 by

$$\mathcal{L}_I = -\frac{g}{\sqrt{2}}(J^\mu W_\mu^+ + J^{\mu\dagger} W_\mu^-) - \left(g \sin \theta_W J_\mu^3 + g' \cos \theta_W \frac{J_\mu^Y}{2}\right) A^\mu - \left(g \cos \theta_W J_\mu^3 - g' \sin \theta_W \frac{J_\mu^Y}{2}\right) Z^\mu \quad (2.27)$$

587 the first term is the weak charged current interaction, while the second term is the

588 electromagnetic interaction under the condition

$$g \sin \theta_W = g' \cos \theta_W = e, \quad \frac{g'}{g} = \tan \theta_W \quad (2.28)$$

589 contained in the eqn.2.25; the third term is the neutral weak current.

590 Note that the neutral fields transformation given by the eqn. 2.26 can be written in

591 terms of the coupling constants  $g$  and  $g'$  as:

$$A_\mu = \frac{g' W_\mu^3 + g B_\mu}{\sqrt{g^2 + g'^2}}, \quad Z_\mu = \frac{g W_\mu^3 - g' B_\mu}{\sqrt{g^2 + g'^2}} \quad (2.29)$$

592 So far, the Lagrangian density describing the non-massive EWI is:

$$\mathcal{L}_{nmEWI} = \mathcal{L}_0 + \mathcal{L}_G \quad (2.30)$$

593 where fermion and gauge fields have been considered massless because their regular

594 mass terms are manifestly non invariant under G transformations; therefore, masses

595 have to be generated in a gauge invariant way. The mechanism by which this goal is

596 achieved is known as the “Higgs mechanism” and is closely connected to the concept  
 597 of “spontaneous symmetry breaking.”

### 598 2.3.1 Spontaneous symmetry breaking

599 Figure 2.6 left shows a steel nail (top) which is subject to an external force; the form  
 of the potential energy is also shown (bottom).

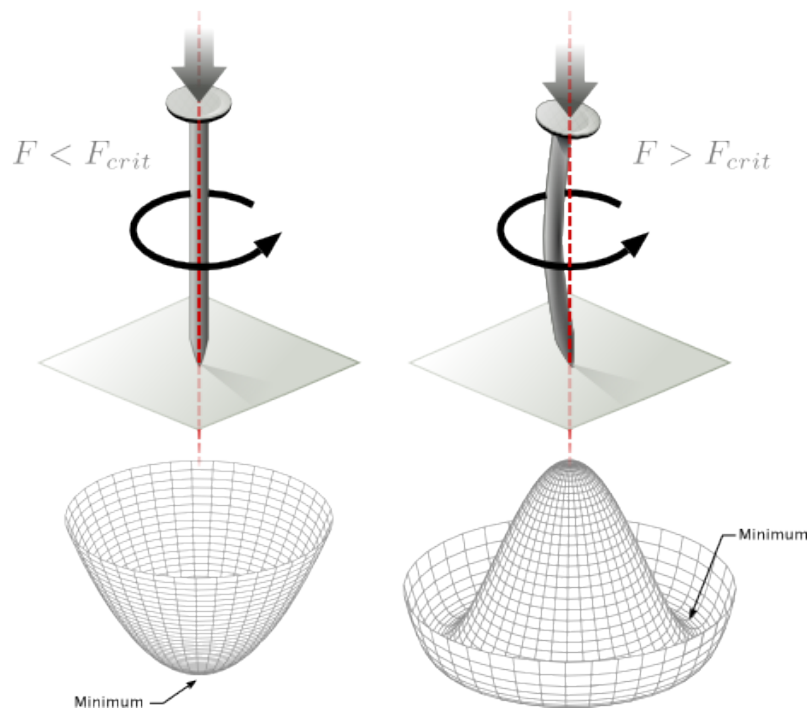


**Figure 2.6:** Spontaneous symmetry breaking mechanism. The steel nail, subject to an external force (top left), has rotational symmetry with respect to its axis. When the external force overcomes a critical value the nail buckles (top right) choosing a minimal energy state (ground state) and thus “*breaking spontaneously the rotational symmetry*”. The potential energy (bottom) changes but holds the rotational symmetry; however, an infinite number of asymmetric ground states are generated and circularly distributed in the bottom of the potential [34].

600  
 601 Before reaching the critical force value, the system has rotational symmetry with re-  
 602 spect to the nail axis; however, after the critical force value is reached the nail buckles  
 603 (top right). The form of the potential energy (bottom right) changes, preserving its

604 rotational symmetry although its minima do not exhibit that rotational symmetry  
 605 any longer. Right before the nail buckles there is no indication of the direction the  
 606 nail will bend because any of the directions are equivalent, but once the nail bent,  
 607 choosing a direction, an arbitrary minimal energy state (ground state) is selected and  
 608 it does not share the system rotational symmetry. This mechanism for reaching an  
 609 asymmetric ground state is known as “*spontaneous symmetry breaking (SSB)*”.  
 610 The lesson from this analysis is that the way to introduce the SSB mechanism into a  
 611 system is by adding the appropriate potential to it.

612

613 Figure 2.7 shows a plot of the potential  $V(\phi)$  in the case of a scalar field  $\phi$

$$V(\phi) = \mu^2 \phi^\dagger \phi + \lambda (\phi^\dagger \phi)^2 \quad (2.31)$$

614 If  $\mu^2 > 0$  the potential has only one minimum at  $\phi = 0$  and describe a scalar field  
 615 with mass  $\mu$ . If  $\mu^2 < 0$  the potential has a local maximum at  $\phi = 0$  and two minima  
 616 at  $\phi = \pm\sqrt{-\mu^2/\lambda}$  which enables the SSB mechanism to work.

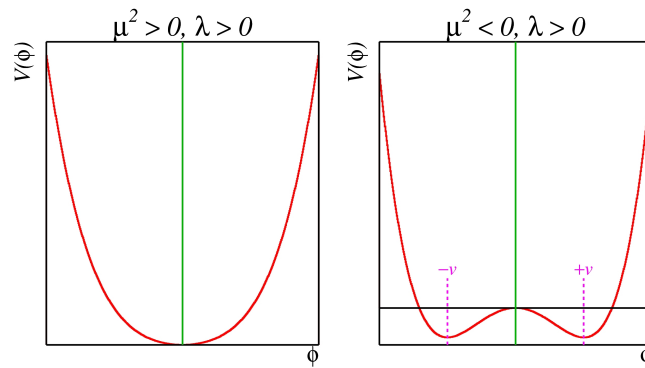


**Figure 2.7:** Shape of the potential  $V(\phi)$  for  $\lambda > 0$  and:  $\mu^2 > 0$  (left) and  $\mu^2 < 0$  (right). The case  $\mu^2 < 0$  corresponds to the potential suitable for introducing the SSB mechanism by choosing one of the two ground states which are connected via reflection symmetry. [34].

617 In the case of a complex scalar field  $\phi(x)$

$$\phi(x) = \frac{1}{\sqrt{2}}(\phi_1 + i\phi_2) \quad (2.32)$$

the Lagrangian (invariant under global  $U(1)$  transformations) is given by

$$\mathcal{L} = (\partial_\mu \phi)^\dagger (\partial^\mu \phi) - V(\phi), \quad V(\phi) = \mu^2 \phi^\dagger \phi + \lambda (\phi^\dagger \phi)^2 \quad (2.33)$$

where an appropriate potential has been added in order to introduce the SSB.

As seen in figure 2.8, the potential has now an infinite number of minima circularly distributed along the  $\xi$ -direction which makes possible the occurrence of the SSB by choosing an arbitrary ground state; for instance,  $\xi = 0$ , i.e.  $\phi_1 = v, \phi_2 = 0$

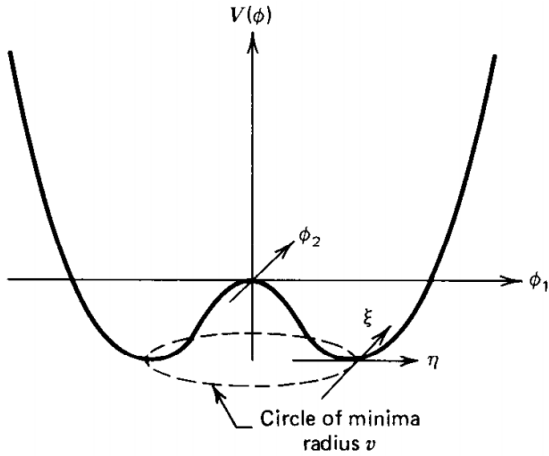


**Figure 2.8:** Potential for complex scalar field. There is a circle of minima of radius  $v$  along the  $\xi$ -direction [3].

$$\phi_0 = \frac{v}{\sqrt{2}} \exp(i\xi) \xrightarrow{\text{SSB}} \phi_0 = \frac{v}{\sqrt{2}} \quad (2.34)$$

As usual, excitations over the ground state are studied by making an expansion about it; thus, the excitation can be parametrized as:

$$\phi(x) = \frac{1}{\sqrt{2}}(v + \eta(x) + i\xi(x)) \quad (2.35)$$

625 which when substituted into eqn. 2.33 produces a Lagrangian in terms of the new  
 626 fields  $\eta$  and  $\xi$

$$\mathcal{L}' = \frac{1}{2}(\partial_\mu \xi)^2 + \frac{1}{2}(\partial_\mu \eta)^2 + \mu^2 \eta^2 - V(\phi_0) - \lambda v \eta (\eta^2 + \xi^2) - \frac{\lambda}{4}(\eta^2 + \xi^2)^2 \quad (2.36)$$

627 where the last two terms represent the interactions and self-interaction between the  
 628 two fields  $\eta$  and  $\xi$ . The particular feature of the SSB mechanism is revealed when  
 629 looking to the first three terms of  $\mathcal{L}'$ . Before the SSB, only the massless  $\phi$  field is  
 630 present in the system; after the SSB there are two fields of which the  $\eta$ -field has  
 631 acquired mass  $m_\eta = \sqrt{-2\mu^2}$  while the  $\xi$ -field is still massless (see figure 2.9).

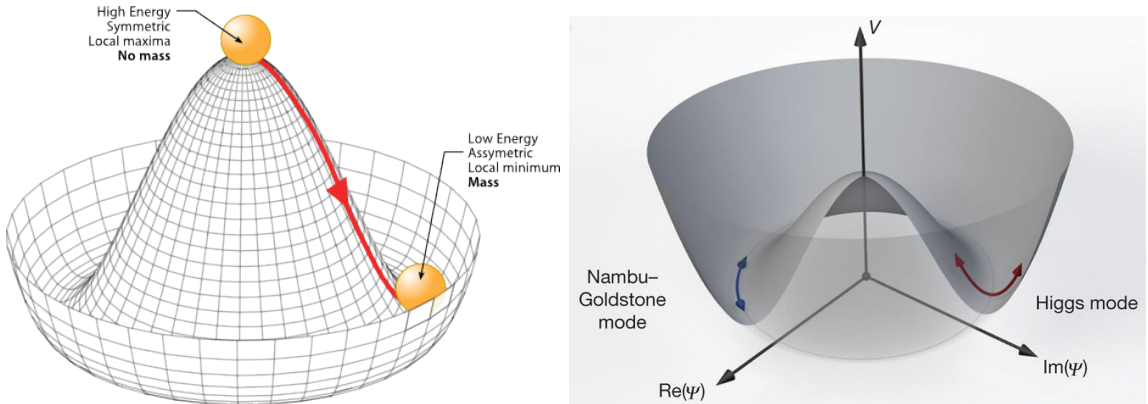


**Figure 2.9:** SSB mechanism for a complex scalar field [34, 35].

632 Thus, the SSB mechanism serves as a method to generate mass but as a side effect a  
 633 massless field is introduced in the system. This fact is known as the Goldstone theorem  
 634 and states that a massless scalar field appears in the system for each continuous  
 635 symmetry spontaneously broken. Another version of the Goldstone theorem states  
 636 that “if a Lagrangian is invariant under a continuous symmetry group  $G$ , but the  
 637 vacuum is only invariant under a subgroup  $H \subset G$ , then there must exist as many  
 638 massless spin-0 particles (Nambu-Goldstone bosons) as broken generators.” [33] The

639 Nambu-Goldstone boson can be understood considering that the potential in the  $\xi$ -  
 640 direction is flat so excitations in that direction are not energy consuming and thus  
 641 represent a massless state.

### 642 2.3.2 Higgs mechanism

643 When the SSB mechanism is introduced in the formulation of the EWI in an attempt  
 644 to generate the mass of the so far massless gauge bosons and fermions, an interesting  
 645 effect is revealed. In order to keep the G symmetry group invariance and generate  
 646 the mass of the EW gauge bosons a G invariant Lagrangian density ( $\mathcal{L}_S$ ) has to be  
 647 added to the non massive EWI Lagrangian (eqn. 2.30)

$$\mathcal{L}_S = (D_\mu \phi)^\dagger (D^\mu \phi) - \mu^2 \phi^\dagger \phi - \lambda (\phi^\dagger \phi)^2, \quad \lambda > 0, \mu^2 < 0 \quad (2.37)$$

$$D_\mu \phi = \left( i\partial_\mu - g \frac{\sigma_i}{2} W_\mu^i - g' \frac{Y}{2} B_\mu \right) \phi \quad (2.38)$$

648  $\phi$  has to be an isospin doublet of complex scalar fields so it preserves the G invariance;  
 649 thus  $\phi$  can be defined as:

$$\phi = \begin{pmatrix} \phi^+ \\ \phi^0 \end{pmatrix} \equiv \frac{1}{\sqrt{2}} \begin{pmatrix} \phi_1 + i\phi_2 \\ \phi_3 + i\phi_4 \end{pmatrix}. \quad (2.39)$$

650 The minima of the potential are defined by

$$\phi^\dagger \phi = \frac{1}{2} (\phi_1^2 + \phi_2^2 + \phi_3^2 + \phi_4^2) = -\frac{\mu^2}{2\lambda}. \quad (2.40)$$

651 The choice of the ground state is critical. By choosing a ground state, invariant under  
 652  $U(1)_{em}$  gauge symmetry, the photon will remain massless and the  $W^\pm$  and  $Z$  bosons  
 653 masses will be generated which is exactly what is needed. In that sense, the best

654 choice corresponds to a weak isospin doublet with  $T_3 = -1/2$ ,  $Y_W = 1$  and  $Q = 0$   
 655 which defines a ground state with  $\phi_1 = \phi_2 = \phi_4$  and  $\phi_3 = v$ :

$$\phi_0 \equiv \frac{1}{\sqrt{2}} \begin{pmatrix} 0 \\ v \end{pmatrix}, \quad v^2 \equiv -\frac{\mu^2}{\lambda}. \quad (2.41)$$

656 where the vacuum expectation value  $v$  is fixed by the Fermi coupling  $G_F$  according  
 657 to  $v = (\sqrt{2}G_F)^{1/2} \approx 246$  GeV.

658 The G symmetry has been broken and three Nambu-Goldstone bosons will appear.  
 659 The next step is to expand  $\phi$  about the chosen ground state as:

$$\phi(x) = \frac{1}{\sqrt{2}} \exp\left(\frac{i}{v} \sigma_i \theta^i(x)\right) \begin{pmatrix} 0 \\ v + H(x) \end{pmatrix} \approx \frac{1}{\sqrt{2}} \begin{pmatrix} \theta_1(x) + i\theta_2(x) \\ v + H(x) - i\theta_3(x) \end{pmatrix} \quad (2.42)$$

660 to describe fluctuations from the ground state  $\phi_0$ . The fields  $\theta_i(x)$  represent the  
 661 Nambu-Goldstone bosons while  $H(x)$  is known as “higgs field.” The fundamental  
 662 feature of the parametrization used is that the dependence on the  $\theta_i(x)$  fields is  
 663 factored out in a global phase that can be eliminated by taking the physical “unitary  
 664 gauge”  $\theta_i(x) = 0$ . Therefore the expansion about the ground state is given by:

$$\phi(x) \frac{1}{\sqrt{2}} \begin{pmatrix} 0 \\ v + H(x) \end{pmatrix} \quad (2.43)$$

665 which when substituted into  $\mathcal{L}_S$  (eqn. 2.37) results in a Lagrangian containing the now  
 666 massive three gauge bosons  $W^\pm, Z$ , one massless gauge boson (photon) and the new  
 667 Higgs field ( $H$ ). The three degrees of freedom corresponding to the Nambu-Goldstone  
 668 bosons are now integrated into the massive gauge bosons as their longitudinal polar-  
 669 izations which were not available when they were massless particles. The effect by  
 670 which vector boson fields acquire mass after an spontaneous symmetry breaking but  
 671 without an explicit gauge invariance breaking is known as the “*Higgs mechanism*.”

672 The mechanism was proposed by three independent groups: F.Englert and R.Brout  
 673 in August 1964 [36], P.Higgs in October 1964 [37] and G.Guralnik, C.Hagen and  
 674 T.Kibble in November 1964 [38]; however, its importance was not realized until  
 675 S.Glashow [14], A.Salam [15] and S.Weinberg [16] independently proposed that elec-  
 676 tromagnetic and weak interactions are two manifestations of a more general interac-  
 677 tion called “electroweak interaction” in 1967.

### 678 2.3.3 Masses of the gauge bosons

679 The mass of the gauge bosons is extracted by evaluating the kinetic part of Lagrangian  
 680  $\mathcal{L}_S$  in the ground state (known also as the vacuum expectation value) i.e.

$$\left| \left( \partial_\mu - ig \frac{\sigma_i}{2} W_\mu^i - i \frac{g'}{2} B_\mu \right) \phi_0 \right|^2 = \left( \frac{1}{2} v g \right)^2 W_\mu^+ W^{-\mu} + \frac{1}{8} v^2 (W_\mu^3, B_\mu) \begin{pmatrix} g^2 & -gg' \\ -gg' & g'^2 \end{pmatrix} \begin{pmatrix} W^{3\mu} \\ B^\mu \end{pmatrix} \quad (2.44)$$

681 comparing with the typical mass term for a charged boson  $M_W^2 W^+ W^-$

$$M_W = \frac{1}{2} v g. \quad (2.45)$$

The second term in the right side of the eqn.2.44 comprises the masses of the neutral  
 bosons, but it needs to be written in terms of the gauge fields  $Z_\mu$  and  $A_\mu$  in order to  
 be compared to the typical mass terms for neutral bosons, therefore using eqn. 2.29

$$\begin{aligned} \frac{1}{8} v^2 [g^2 (W_\mu^3)^2 - 2gg' W_\mu^3 B^\mu + g'^2 B_\mu^2] &= \frac{1}{8} v^2 [g W_\mu^3 - g' B_\mu]^2 + 0[g' W_\mu^3 + g B_\mu]^2 \quad (2.46) \\ &= \frac{1}{8} v^2 [\sqrt{g^2 + g'^2} Z_\mu]^2 + 0[\sqrt{g^2 + g'^2} A_\mu]^2 \end{aligned}$$

682 and then

$$M_Z = \frac{1}{2}v\sqrt{g^2 + g'^2}, \quad M_A = 0 \quad (2.47)$$

### 683 2.3.4 Masses of the fermions

684 The lepton mass terms can be generated by introducing a gauge invariant Lagrangian  
 685 term describing the Yukawa coupling between the lepton field and the Higgs field:

$$\mathcal{L}_{Yl} = -G_l \left[ (\bar{\nu}_l, \bar{l})_L \begin{pmatrix} \phi^+ \\ \phi^0 \end{pmatrix} l_R + \bar{l}_R (\phi^-, \bar{\phi}^0) \begin{pmatrix} \nu_l \\ l \end{pmatrix} \right], \quad l = e, \mu, \tau. \quad (2.48)$$

686 After the SSB and replacing the usual field expansion about the ground state (eqn.2.41)  
 687 into  $\mathcal{L}_{Yl}$ , the mass term arises

$$\mathcal{L}_{Yl} = -m_l(\bar{l}_L l_R + \bar{l}_R l_L) - \frac{m_l}{v}(\bar{l}_L l_R + \bar{l}_R l_L)H = -m_l \bar{l}l \left(1 + \frac{H}{v}\right) \quad (2.49)$$

688

$$m_l = \frac{G_l}{\sqrt{2}}v \quad (2.50)$$

689 where the additional term represents the lepton-Higgs interaction. The quark masses  
 690 are generated in a similar way as lepton masses but for the upper member of the  
 691 quark doublet a different Higgs doublet is needed:

$$\phi_c = -i\sigma_2\phi^* = \begin{pmatrix} -\bar{\phi}^0 \\ \phi^- \end{pmatrix}. \quad (2.51)$$

692 Additionally, given that the quark isospin doublets are not constructed in terms of  
 693 the mass eigenstates but in terms of the flavor eigenstates as shown in table2.4, the  
 694 coupling parameters will be related to the CKM matrix elements; thus the quark  
 695 Lagrangian is given by:

$$\mathcal{L}_{Yq} = -G_d^{i,j}(\bar{u}_i, \bar{d}'_i)_L \begin{pmatrix} \phi^+ \\ \phi^0 \end{pmatrix} d_{jR} - G_u^{i,j}(\bar{u}_i, \bar{d}'_i)_L \begin{pmatrix} -\bar{\phi}^0 \\ \phi^- \end{pmatrix} u_{jR} + h.c. \quad (2.52)$$

696 with  $i,j=1,2,3$ . After SSB and expansion about the ground state, the diagonal form  
 697 of  $\mathcal{L}_{Yq}$  is:

$$\mathcal{L}_{Yq} = -m_d^i \bar{d}_i d_i \left(1 + \frac{H}{v}\right) - m_u^i \bar{u}_i u_i \left(1 + \frac{H}{v}\right) \quad (2.53)$$

698 Fermion masses depends on arbitrary couplings  $G_l$  and  $G_{u,d}$  and are not predicted  
 699 by the theory.

### 700 2.3.5 The Higgs field

701 After the characterization of the fermions and gauge bosons as well as their inter-  
 702 actions, it is necessary to characterize the Higgs field itself. The Lagrangian  $\mathcal{L}_S$  in  
 703 eqn:2.37 written in terms of the gauge bosons is given by

$$\mathcal{L}_S = \frac{1}{4} \lambda v^4 + \mathcal{L}_H + \mathcal{L}_{HV} \quad (2.54)$$

$$704 \quad \mathcal{L}_H = \frac{1}{2} \partial_\mu H \partial^\mu H - \frac{1}{2} m_H^2 H^2 - \frac{1}{2v} m_H^2 H^3 - \frac{1}{8v^2} m_H^2 H^4 \quad (2.55)$$

$$705 \quad \mathcal{L}_{HV} = m_H^2 W_\mu^+ W^{\mu-} \left(1 + \frac{2}{v} H + \frac{2}{v^2} H^2\right) + \frac{1}{2} m_Z^2 Z_\mu Z^\mu \left(1 + \frac{2}{v} H + \frac{2}{v^2} H^2\right) \quad (2.56)$$

706 The mass of the Higgs boson is deduced as usual from the mass term in the Lagrangian  
 707 resulting in:

$$m_H = \sqrt{-2\mu^2} = \sqrt{2\lambda}v \quad (2.57)$$

708 however, it too is not predicted by the theory. The experimental efforts to find the  
 709 Higgs boson, carried out by the CMS and ATLAS experiments<sup>8</sup>, gave great results

---

<sup>8</sup> CMS stands for Compact Muon Solenoid; ATLAS stand for A Toroidal LHC Apparatus. Both are general experiments held at the Large Hadron Collider(LHC)

710 by July of 2012 when the discovery of a new particles was announced and which  
 711 is compatible with the Higgs boson predicted by the electroweak theory [39, 40].  
 712 Although at the announcement time there were some reservations about calling the  
 713 new particle the “Higgs boson”, today this name is widely accepted. The result of  
 714 the measurement of the Higgs mass reported by both experiments [41] is in table 2.7.

Property	Value
Electric charge	0
Colour charge	0
Spin	0
Weak isospin	-1/2
Weak hypercharge	1
Parity	1
Mass ( $\text{GeV}/c^2$ )	$125.09 \pm 0.21 \text{ (stat.)} \pm 0.11 \text{ (syst.)}$

**Table 2.7:** Higgs boson properties. Higgs mass is not predicted by the theory and the value here corresponds to the experimental measurement.

715

### 716 2.3.6 Higgs boson production mechanisms at LHC.

717 At LHC, Higgs boson is produced as a result of the collision of two counter-rotating  
 718 protons beams. A detailed description of the LHC machine will be presented in the  
 719 chapter 3. “The total cross section” is the parameter that quantify the number of pp  
 720 collisions that happen when a number of protons are fired at each other. Different  
 721 results can be obtained after a pp collision and for each one the “cross section” is  
 722 defined as the number of pp collisions that conclude in that particular result with  
 723 respect to the number of protons fired at each other.

724 Protons are composed of quarks and these quarks are bound by gluons; however, what  
 725 is commonly called the quark content of the proton makes reference to the valence  
 726 quarks. A sea of quarks and gluons is also present inside the proton as represented  
 727 in figure 2.10. In a proton-proton (pp) collision, the constituents (quarks and gluons)

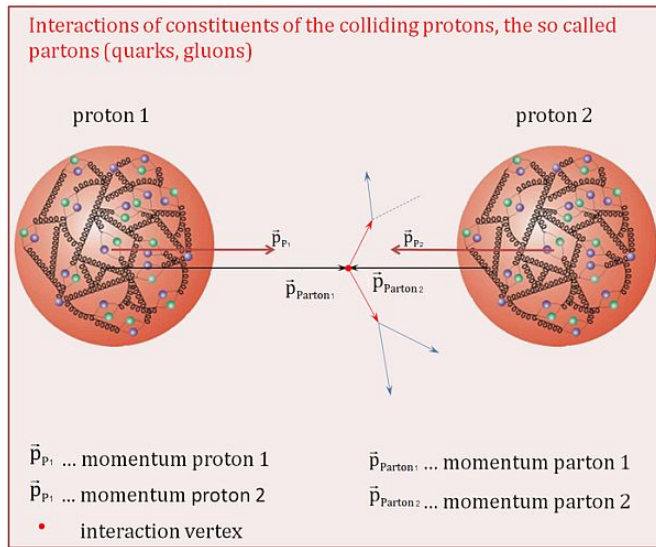


**Figure 2.10:** Proton-proton collision. Protons are composed of 3 valence quarks, a sea of quarks and gluons; therefore in a proton-proton collision, quarks and gluons are those who collide. [45].

are those who collide. The pp cross section depends on the momentum of the colliding particles, reason for which it is needed to know how the momentum is distributed inside the proton. Quarks and gluons are known as partons and the functions that describes how the proton momentum is distributed among partons inside it are called “parton distribution functions (PDFs)”; PDFs are determined from experimental data obtained in experiments where the internal structure of hadrons is tested.

In addition, in physics, a common approach to study complex systems consist in starting with a simpler version of them, for which a well known description is available, and add an additional “perturbation” which represent a small deviation from the known behavior. If the perturbation is small enough, the physical quantities associated with the perturbed system are expressed as a series of corrections to those of the simpler system; therefore, the more terms are considered in the series (the higher order in the perturbation series), the more precise is the the description of the complex system.

742 This thesis explore the Higgs production at LHC; therefore the overview presented  
 743 here will be oriented specifically to the production mechanisms after pp collisions at  
 744 LHC.

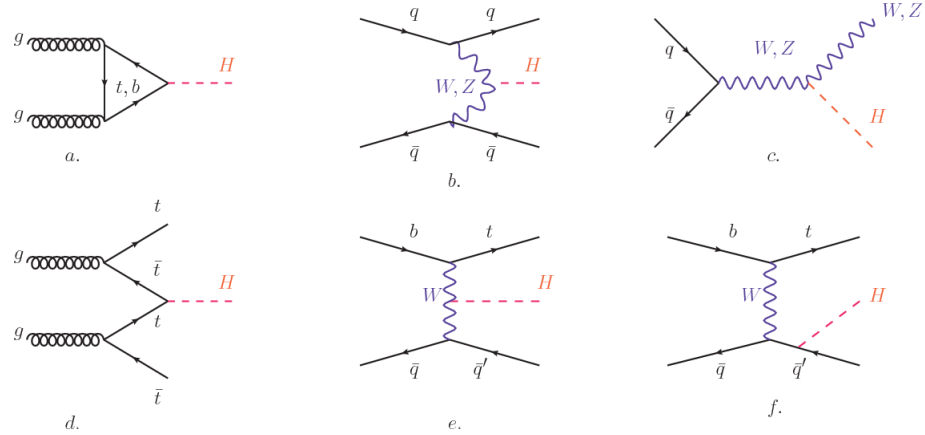


**Figure 2.11:** Main Higgs production mechanism Feynman diagrams. a. gluon-gluon fusion, b. vector boson fusion (VBF), c. Higgs-strahlung, d. Associated production with a top or bottom quark pair, e-f. associated production with a single top quark.

745 Figure 2.11 shows the Feynman diagrams for the leading order (first order) Higgs  
 746 production processes at LHC, while the cross section for Higgs production as a func-  
 747 tion of the center of mass-energy ( $\sqrt{s}$ ) for pp collisions is showed in figure 2.12 left.  
 748 The tags NLO (next to leading order), NNLO (next to next to leading order) and  
 749 N3LO (next to next to next to leading order) make reference to the order at which  
 750 the perturbation series has been considered.

751 As shown in eqns 2.48, 2.52 and 2.56, the strength of the Higgs-fermion interaction  
 752 is proportional to the fermion mass while the strength of the Higgs-gauge boson  
 753 interaction is proportional to the square of the gauge boson mass, which implies  
 754 that the Higgs production and decay mechanisms are dominated by couplings  $H -$   
 755  $(W, Z, t, b, \tau)$ .

756 The main production mechanism is the gluon fusion (figure 2.11a and  $pp \rightarrow H$  in figure  
 757 2.12) given that gluons carry the highest fraction of momentum of the protons in pp

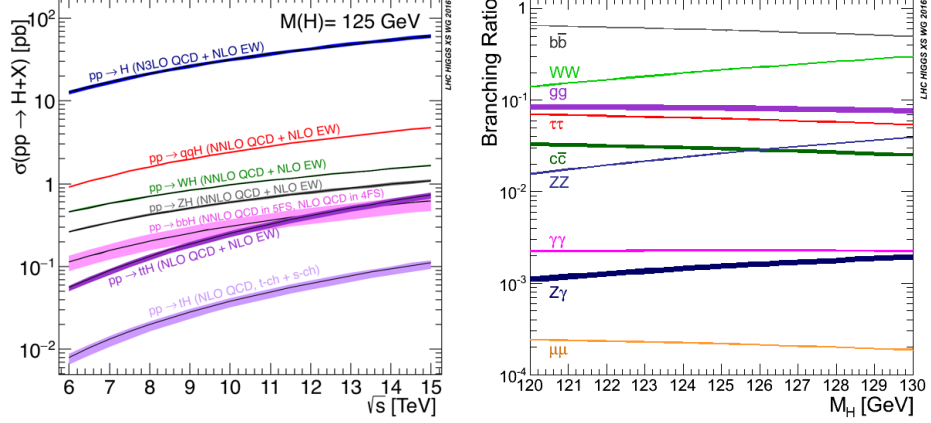


**Figure 2.12:** Higgs production cross sections (left) and decay branching ratios (right) for the main mechanisms. The VBF is indicated as  $qqH$  [42].

colliders. Since the Higgs boson does not couple to gluons, the mechanism proceeds through the exchange of a virtual top-quark loop given that for it the coupling is the biggest. Note that in this process, the Higgs boson is produced alone, which makes this mechanism experimentally clean when combined with the two-photon or the four-lepton decay channels (see section 2.3.7).

Vector boson fusion (figure 2.11b and  $pp \rightarrow qqH$  in figure 2.12) has the second largest production cross section. The scattering of two fermions is mediated by a weak gauge boson which later emits a Higgs boson. In the final state, the two fermions tend to be located in a particular region of the detector which is used as a signature when analyzing the datasets provided by the experiments. More details about how to identify events of interest in an analysis will be given in chapter 4.

The next production mechanism is Higgs-strahlung (figure 2.11c and  $pp \rightarrow WH, pp \rightarrow ZH$  in figure 2.12) where two fermions annihilate to form a weak gauge boson. If the initial fermions have enough energy, the emergent boson eventually will emit a Higgs boson.

The associated production with a top or bottom quark pair and the associated pro-

duction with a single top quark (figure 2.11d-f and  $pp \rightarrow bbH, pp \rightarrow t\bar{t}H, pp \rightarrow tH$  in figure 2.12) have a smaller cross section than the main three mechanisms above, but they provide a good opportunity to test the Higgs-top coupling. The analysis reported in this thesis is developed using these production mechanisms. A detailed description of the  $tH$  mechanism will be given in section 2.4.

### 2.3.7 Higgs decay channels

When a particle can decays through several modes, also known as channels, the probability of decaying through a given channel is quantified by the “branching ratio (BR)” of the decay channel; thus, the BR is defined as the ratio of number of decays going through that given channel to the total number of decays. In regard to the Higgs boson decay, the BR can be predicted with accuracy once the Higgs mass is known [43, 44]. In figure 2.12 right, a plot of the BR as a function of the Higgs mass is presented. The largest predicted BR corresponds to the  $b\bar{b}$  pair decay channel (see table 2.8).

Decay channel	Branching ratio	Rel. uncertainty
$H \rightarrow b\bar{b}$	$5.84 \times 10^{-1}$	$+3.2\% - 3.3\%$
$H \rightarrow W^+W^-$	$2.14 \times 10^{-1}$	$+4.3\% - 4.2\%$
$H \rightarrow \tau^+\tau^-$	$6.27 \times 10^{-2}$	$+5.7\% - 5.7\%$
$H \rightarrow ZZ$	$2.62 \times 10^{-2}$	$+4.3\% - 4.1\%$
$H \rightarrow \gamma\gamma$	$2.27 \times 10^{-3}$	$+5.0\% - 4.9\%$
$H \rightarrow Z\gamma$	$1.53 \times 10^{-3}$	$+9.0\% - 8.9\%$
$H \rightarrow \mu^+\mu^-$	$2.18 \times 10^{-4}$	$+6.0\% - 5.9\%$

**Table 2.8:** Predicted branching ratios and the relative uncertainty for a SM Higgs boson with  $m_H = 125\text{GeV}/c^2$ . [21]

789 **2.4 Associated Production of Higgs Boson and**  
 790 **Single Top Quark.**

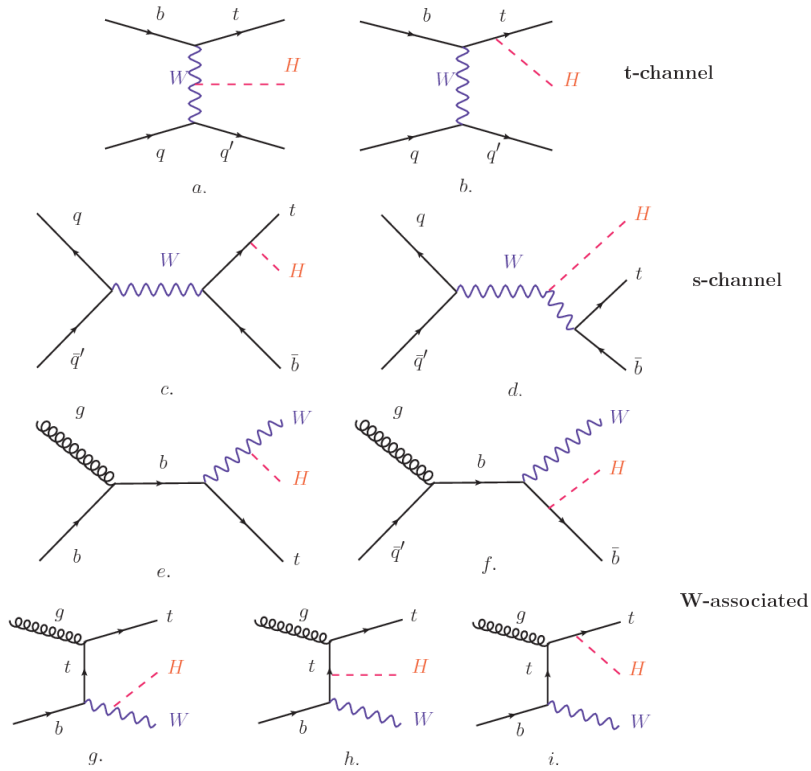


**Figure 2.13:** Associated higgs production mechanism Feynman diagrams. a.,b. t-channel (tHq), c.,d. s-channel (tHb), e-i. W-associated.

791 Associated production of Higgs boson have been extensively studied [46–50]. While  
 792 measurements of the main Higgs production mechanisms rates are sensitive to the  
 793 strength of the Higgs coupling to W boson or top quark, they are not sensitive to the  
 794 relative sign between the two couplings. In this thesis, the Higgs boson production  
 795 mechanism explored is the associated production with a single top quark (*th*) which  
 796 offers sensitiveness to the relative sign of the Higgs couplings to W boson and to top  
 797 quark. The description given here is based on the reference [48]

799 A process where two incoming particles interact and produce a final state with two  
 800 particles can proceed in three ways also called channels (see, for instance, figure 2.13  
 801 ommiting the red line). The t-channel represents processes where an intermediate  
 802 particle is emitted by one of the incoming particles and absorbed by the other. The  
 803 s-channel represent processes where the two incoming particles merge into an inter-  
 804 mediate particle which eventually will split into the particles in the final state. The  
 805 third channel, u-channel, is similar to the t-channel but the two outgoing particles  
 806 interchange their roles.

807

808 The  $tH$  production where Higgs boson can be radiated either from the top quark or  
 809 from the W boson is represented by the leading order Feynman diagrams in figure  
 810 2.13. The cross section for the  $tH$  process is calculated, as usual, summing over  
 811 the contributions from the different feynman diagrams; therefore it depends on the  
 812 interference between the contributions. In the SM, the interference for t-channel ( $tHq$   
 813 process) and W-associated ( $tHW$  process) production is destructive [46] resulting in  
 814 the small cross sections presented in table 2.9.

tH production channel	Cross section (fb)
t-channel ( $pp \rightarrow tHq$ )	$70.79^{+2.99}_{-4.80}$
W-associated ( $pp \rightarrow tHW$ )	$15.61^{+0.83}_{-1.04}$
s-channel( $pp \rightarrow tHb$ )	$2.87^{+0.09}_{-0.08}$

**Table 2.9:** Predicted SM cross sections for  $tH$  production at  $\sqrt{s} = 13$  TeV [51, 52].

815

816 While the s-channel contribution can be neglected, it will be shown that a deviation  
 817 from the SM destructive interference would result in an enhancement of the  $tH$  cross  
 818 section compared to that in SM, which could be used to get information about the

819 sign of the Higgs-top coupling [48, 49]. In order to describe  $th$  production processes,  
 820 Feynman diagram 2.13b will be considered; there, the W boson is radiated by a  
 821 quark in the proton and eventually it will interact with the b quark. In the high  
 822 energy regime, the effective W approximation [53] allows to describe the process as  
 823 the emmision of an approximately on-shell W and its hard scattering with the b  
 824 quark; i.e.  $Wb \rightarrow th$ . The scattering amplitude for the process is given by

$$\mathcal{A} = \frac{g}{\sqrt{2}} \left[ (C_t - C_V) \frac{m_t \sqrt{s}}{m_W v} A \left( \frac{t}{s}, \varphi; \xi_t, \xi_b \right) + \left( C_V \frac{2m_W s}{v} \frac{1}{t} + (2C_t - C_V) \frac{m_t^2}{m_W v} \right) B \left( \frac{t}{s}, \varphi; \xi_t, \xi_b \right) \right], \quad (2.58)$$

825 where  $C_V \equiv g_{HVV}/g_{HVV}^{SM}$  and  $C_t \equiv g_{Ht}/g_{Ht}^{SM}$  are scaling factors that quantify possible  
 826 deviations of the couplings, Higgs-Vector boson (H-W) and Higgs-top (H-t) respec-  
 827 tively, from the SM couplings;  $s = (p_W + p_b)^2$ ,  $t = (p_W - p_H)^2$ ,  $\varphi$  is the Higgs azimuthal  
 828 angle around the  $z$  axis taken parallel to the direction of motion of the incoming W;  
 829 A and B are funtions describing the weak interaction in terms of the chiral states of  
 830 the quarks b and t. Terms that vanish in the high energy limit have been neglected  
 831 as well as the Higgs and b quark masses<sup>9</sup>.

832 The scattering amplitude grows with energy like  $\sqrt{s}$  for  $C_V \neq C_t$ , in contract to  
 833 the SM ( $C_t = C_V = 1$ ) where the first term in 2.58 cancels out and the amplitude  
 834 is constant for large s; therefore, a deviation from the SM predictions represent an  
 835 enhancement in the  $tHq$  cross section. In particular, for a SM H-W coupling and  
 836 a H-t coupling of inverted sigh with respect to the SM ( $C_V = -C_t = 1$ ) the  $tHq$   
 837 cross section is enhanced by a factor greater 10 as seen in the figure 2.14 taken from  
 838 reference [48]; reference [54] have reported similar enhancement results.  
 839 A similar analysis is valid for the W-associated channel but, in that case, the inter-

---

<sup>9</sup> A detailed explanation of the structure and approximations used to derive  $\mathcal{A}$  can be fount in reference [48]

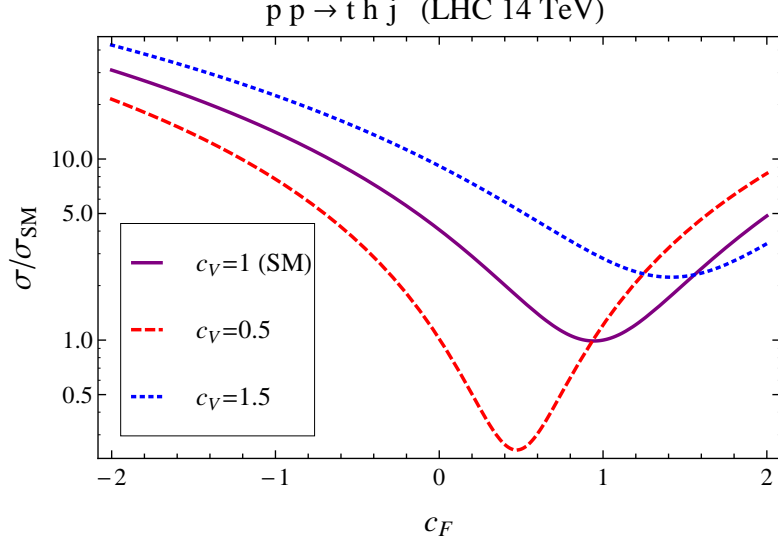


**Figure 2.14:** Cross section for  $tHq$  process as a function of  $C_t$ , normalized to the SM, for three values of  $C_V$ . In the plot  $C_f$  refers to the Higgs-fermion coupling which is dominated by the H-t coupling  $C_t$ . Solid, dashed and dotted lines correspond to  $C_V = 1, 0.5, 1.5$  respectively. Note that for the SM ( $C_V = C_t = 1$ ), the destructive effect of the interference is maximal.

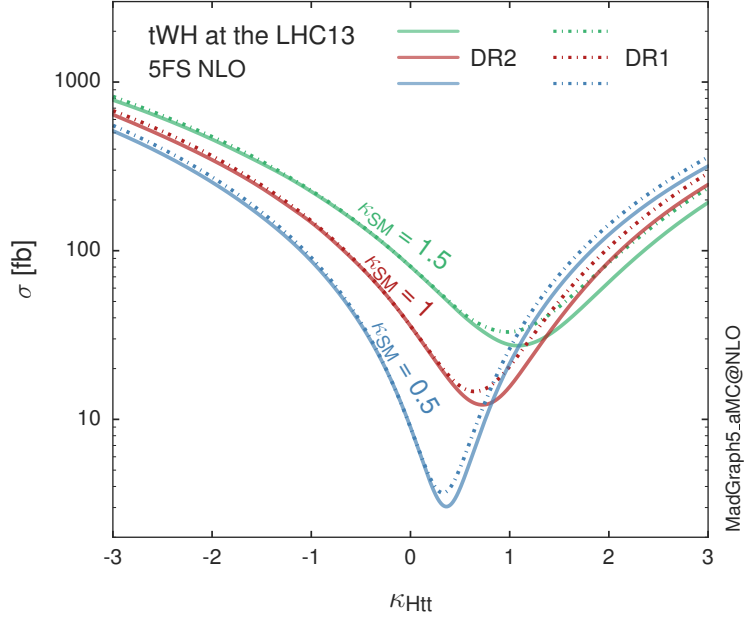


**Figure 2.15:** Cross section for  $tHW$  process as a function of  $\kappa_{Htt}$ , for three values of  $\kappa_{SM}$  at  $\sqrt{s} = 13$  TeV.  $\kappa_{Htt}^2 = \sigma_{Htt}/\sigma_{Htt}^{SM}$  is a simple rescaling of the SM Higgs interactions.

ference is more complicated since there are more than two contributions and an additional interference with the production of Higgs boson and a top pair process( $t\bar{t}H$ ). The calculations are made using the so-called Diagram Removal (DR) technique where interfering diagrams are removed (or added) from the calculations in order to evaluate the impact of the removed contributions. DR1 was defined to neglect  $t\bar{t}H$  interference while DR2 was defined to take  $t\bar{t}H$  interference into account [55]. As shown in figure 2.15, the  $tHW$  cross section is enhanced from about 15 fb (SM:  $\kappa_{Htt} = 1$ ) to about 150 fb ( $\kappa_{Htt} = -1$ ). Differences between curves for DR1 and DR2 help to gauge the impact of the interference with  $t\bar{t}H$ . Results of the calculations of the  $tHq$  and  $tHW$  cross sections at  $\sqrt{s} = 13$  TeV can be found in reference [56] and a summary of the results is presented in table 2.11.

	$\sqrt{s}$ TeV	$C_t = 1$	$C_t = -1$
$\sigma^{LO}(tHq)(fb)$ [48]	8	$\approx 17.4$	$\approx 252.7$
	14	$\approx 80.4$	$\approx 1042$
$\sigma^{NLO}(tHq)(fb)$ [48]	8	$18.28^{+0.42}_{-0.38}$	$233.8^{+4.6}_{-0.0}$
	14	$88.2^{+1.7}_{-0.0}$	$982.8^{+28}_{-0.0}$
$\sigma^{LO}(tHq)(fb)$ [54]	14	$\approx 71.8$	$\approx 893$
$\sigma^{LO}(tHW)(fb)$ [54]	14	$\approx 16.0$	$\approx 139$
$\sigma^{NLO}(tHq)(fb)$ [56]	8	$18.69^{+8.62\%}_{-17.13\%}$	-
	13	$74.25^{+7.48\%}_{-15.35\%}$	$848^{+7.37\%}_{-13.70\%}$
	14	$90.10^{+7.34\%}_{-15.13\%}$	$1011^{+7.24\%}_{-13.39\%}$
$\sigma^{LO}(tHW)(fb)$ [55]	13	$15.77^{+15.91\%}_{-15.76\%}$	-
$\sigma^{NLO}DR1(tHW)(fb)$ [55]	13	$21.72^{+6.52\%}_{-5.24\%}$	$\approx 150$
$\sigma^{NLO}DR2(tHW)(fb)$ [55]	13	$16.28^{+7.34\%}_{-15.13\%}$	$\approx 150$

**Table 2.10:** Predicted enhancement of the  $tHq$  and  $tHW$  cross sections at LHC for  $C_V = 1$  and  $C_t = \pm 1$  at LO and NLO; the cross section enhancement of more than a factor of 10 is due to the flippling in the sign of the H-t coupling with respect to the SM one.

852 **2.5 The CP-mixing phase**

853 **Chapter 3**

854 **The CMS experiment at the LHC**

855 **3.1 Introduction**

856 Located in the Swiss-French border, the European Council for Nuclear Research  
857 (CERN) is the largest scientific organization leading the particle physics research.  
858 About 13000 people in a broad range of fields including users, students, scientists,  
859 engineers among others, contribute to the data taking and analysis, with the goal  
860 of unveiling the secrets of the nature and revealing the fundamental structure of the  
861 universe. CERN is also the home of the Large Hadron Collider (LHC), the largest  
862 circular particle accelerator around the world, where protons (or heavy ions) traveling  
863 close to the speed of light, are made to collide. These collisions open a window to  
864 investigate how particles (and their constituents if they are composite) interact with  
865 each other, providing clues about the laws of the nature.

866 LHC can run in three modes depending on the particles being accelerated

- 867     • Proton-Proton collisions (pp) multiple physics experiments .  
868     • Lead-Lead collisions (Pb-Pb) Heavy ion experiments.

- 869       • Proton-Lead collisions (p-Pb).

870   Figure 3.1 show an overview of the CERN accelerating complex. There are several  
 871   accelerating stages before the injection to the LHC ring. In the pp mode, after  
 872   removing the electrons from hydrogen atoms in a bottle, protons are accelerated  
 873   in the LINAC2 to 50 MeV and then injected into the proton synchrotron booster  
 874   (BOOSTER) to reach 1.4 GeV in energy. The next boost is provided at the proton  
 875   synchrotron (PS) up to 26 GeV, followed by the injection into the super proton  
 876   synchrotron (SPS) where protons are accelerated to 450 GeV. Finally, protons are  
 877   injected into the LHC where they are accelerated to the target energy of 6.5 TeV. In  
 878   the Pb-Pb mode, the Lead ions are first accelerated in the LINAC3 and then passed as  
 879   long pulses to the Low energy ion ring (LEIR) to be converted into short and dense  
 880   bunches, each containing  $7 \times 10^7$  lead ions. LEIR accelerate the bunches from 4.2  
 881   MeV to 72 MeV. The ions are then passed to the PS to follow the rest of acceleration  
 882   process up to 2.8TeV/n en the LHC ring.

883   **3.2 The LHC**

884   The LHC is a 27 km ring composed of superconducting magnets and accelerating  
 885   structures (among other components) which boost the particles traveling inside it.  
 886   It is installed in the same tunnel where the large Electron-Positron (LEP) collider  
 887   was located, taking advantage of the existing infraestructure as shown in Figure 3.2.  
 888   Two particle beams travel counter-rotating in two separated beam pipes kept at ultra  
 889   high vacuum. In 2008, the first set of collisions involved protons with center-of-mass  
 890   energy of 7 TeV after which the energy was increased to 8 TeV in 2012 and to 13 TeV  
 891   in 2015.

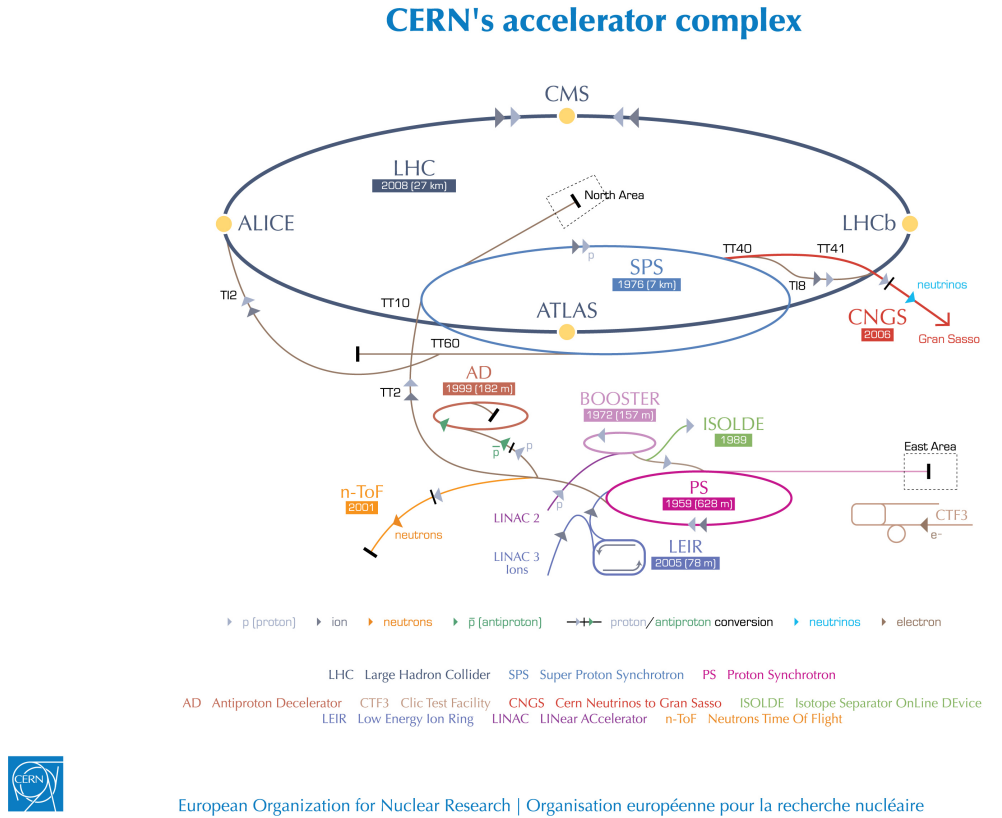
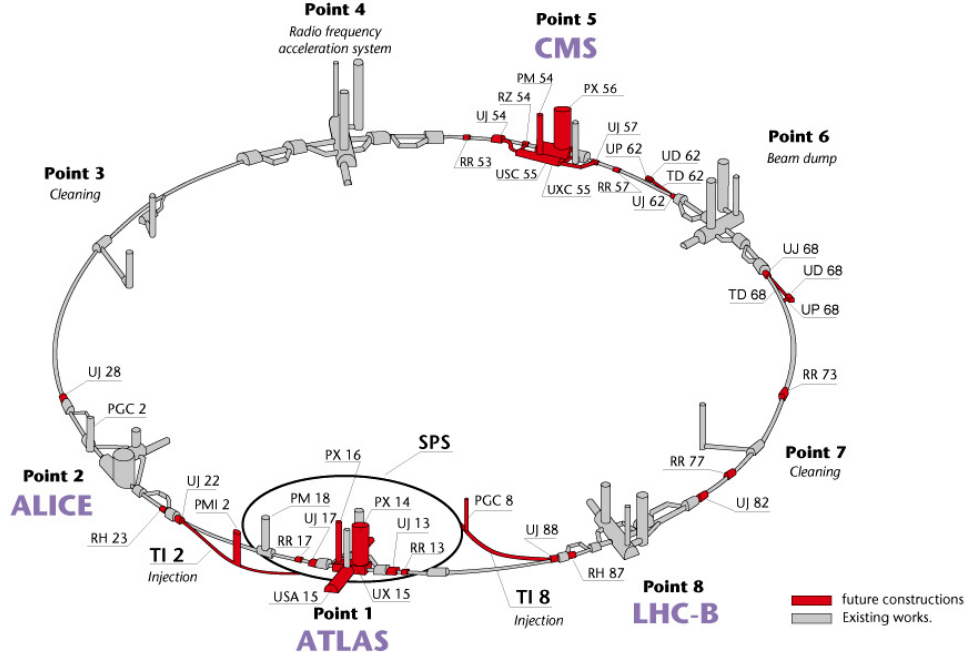


**Figure 3.1:** ref. C.Lefevre, “The CERN accelerator complex,” (2008). CERN-DI-0812015.

892 In order to keep the protons in the circular trajectory carrying that amount of  
 893 energy, strong magnetic fields are needed, bringing the superconductivity into scene.  
 894 The superconducting dipole magnets used in LHC are made of a NbTi alloy, capable  
 895 of transporting currents of about 12000 A when cooled at a temperature below 2K by  
 896 using liquid helium; that current generates a magnetic fields of 8.3 T. Figure 3.3 shows  
 897 the transverse view of the LHC dipole magnets. Additionally, quadrupole magnets  
 898 are used to focus the beam and some other magnetic multipoles are used to correct  
 899 effects generated by the interaction among protons in the beam as well as interactions  
 900 within the beam pipe.  
 901 Regarding to the longitudinal acceleration of the protons, a system of 16 radio-  
 902 frecuency cavities (RF) (8 per beam) is used to accelerate protons. Inside the cavities,

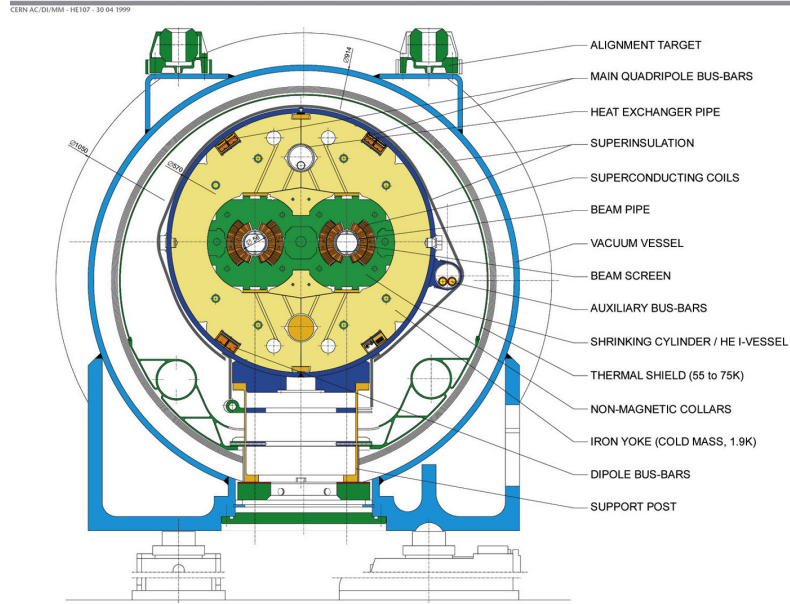
**Layout of the LEP tunnel including future LHC infrastructures.**



CERN AC \_ hf238 \_ V02/02/98

**Figure 3.2:** ref. J.-L. Caron , “Layout of the LEP tunnel including future LHC infrastructures.. L’ensemble du tunnel LEP avec les futures infrastructures LHC.”, <https://cds.cern.ch/record/841542> (Nov, 1993). AC Collection. Legacy of AC. Pictures from 1992 to 2002..

903 the electromagnetic waves become resonant transferring the maximum energy to the  
 904 particle flight through it. Cavities are cooled at 4.5 K. On LHC the RF oscillation  
 905 frecuency is 400MHz and the protons are carefully timed so additionally to the ac-  
 906 celeration effect the bunch structure of the beam is preserved. The Beam is made  
 907 of 2808 “bunches” which are packages of  $1.15 \times 10^{11}$  protons ???. If LHC is at full  
 908 energy, protons with the right energy does not feel any accelerating force but those  
 909 with a different energy will be accelerated or decelerated to keep them in the bunch.  
 910 The paths followed by particles during the acceleration process are shown in Figure  
 911 3.1.

**LHC DIPOLE : STANDARD CROSS-SECTION**


**Figure 3.3:** ref. ACTeam, “Diagram of an LHC dipole magnet. Schéma d’un aimant dipôle du LHC,” (1999). CERN-DI-9906025.

912 Once the beams reach the desired energy, they are brought to cross each other  
 913 producing proton-proton collisions. The bunch crossing happens in precise places  
 914 where the LHC experiments are located. As seen in Figure 3.2, it was needed to  
 915 build the caverns for CMS and ATLAS as well as some additional facilities, but  
 916 most of the initial LEP infrastructure has been used to allocate additional collision  
 917 points. The highest luminosity is delivered at the CMS (point 5) and ATLAS (point  
 918 1) experiments, which are general purpose experiments, enabled to explore physics  
 919 in any of the collision modes. LHCb (point 8) experiment is optimized to explore  
 920 B-physics, while ALICE (point 2) is optimized for heavy ion collisions researches;  
 921 TOTEM (point 5) and LHCf (point 1) are dedicated to forward physics studies and  
 922 MoEDAL (point 8) is intended for monopoles or massive pseudo stable particles  
 923 studies.

### 924 3.3 The CMS experiment

925 The Compact Muon Solenoid (CMS) is a general purpose detector designed to conduct  
926 research in a wide range of physics from standard model to new physics like extra  
927 dimensions and dark matter. Located at the point 5 in the LHC layout as shown in  
928 Figure 3.2, CMS is composed by several detection systems distributed in a cylindrical  
929 structure where the main feature is a solenoid magnet made of superconducting cable  
930 capable to generate a 3.8 T magnetic field. In total, CMS weight about 14000 tons  
931 in a very compact 21.6 m long and 14.6 m diameter cylinder (include areference for  
932 CMS TDR). It was built in 15 separated sections at the ground level and lowered  
933 to the cavern individually to be assembled. Figure 3.4 show the layout of the CMS  
934 detector (CMS TDR).

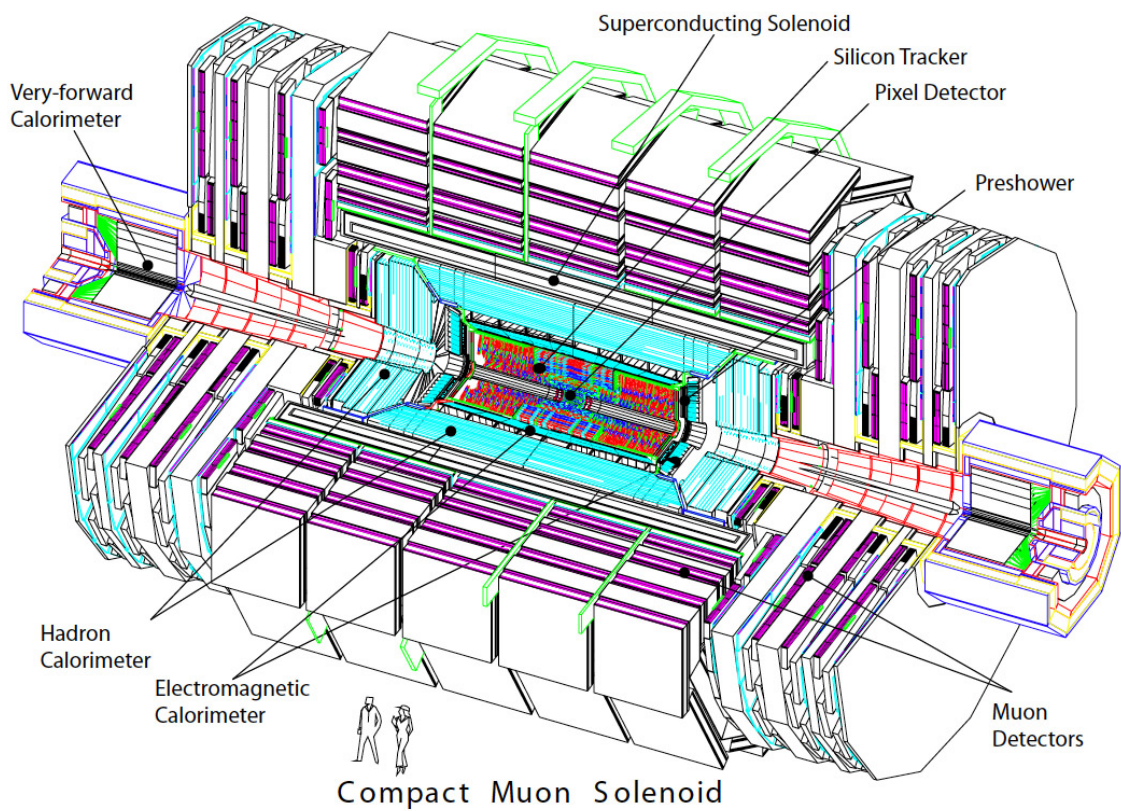


**Figure 3.4:** ref: CMS Collaboration, “Detector Drawings”, CMS-PHO-GEN-2012-002, <http://cds.cern.ch/record/1433717>, 2012.

## 935 Chapter 4

936 Search for production of a Higgs

937 boson and a single top quark in

938 multilepton final states in pp

939 collisions at  $\sqrt{s} = 13$  TeV

### 940 4.1 Introduction

941 This chapter present the search for the associated production of a Higgs boson and  
942 a single top quark events with three leptons in the final state, targeting Higgs decay  
943 modes to  $WW$ ,  $ZZ$ , and  $\tau\tau$ . The analysis uses the 13 TeV dataset produced in 2016,  
944 corresponding to an integrated luminosity of  $35.9\text{fb}^{-1}$ . It is based on and expands  
945 previous analyses at 8 TeV [57, 58] and searches for associated production of  $t\bar{t}$  and  
946 Higgs in the same channel [59], and complements searches in other decay channels  
947 targeting  $H \rightarrow b\bar{b}$  [60].

948 The production cross section of the single top plus Higgs boson ( $tHq$ ) process

949 is driven by a destructive interference of two main diagrams (see Fig. 4.1), where  
 950 the Higgs couples to either the W boson or the top quark. Any deviation from the  
 951 standard model (SM) in the Higgs coupling structure could therefore lead to a large  
 952 enhancement of the cross section, making this analysis sensitive to such deviations.  
 953 A second process, where the Higgs and top quark are accompanied by a W boson  
 954 ( $tHW$ ) has similar behavior, albeit with a weaker interference pattern.

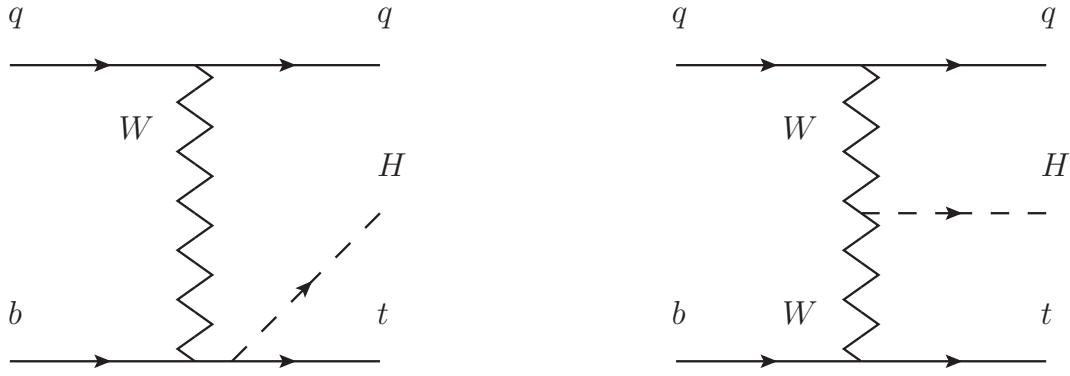


**Figure 4.1:** The two leading-order diagrams of  $tHq$  production.

955 We select events with three leptons and a  $b$  tagged jet in the final state. The  $tHq$   
 956 signal contribution is then determined in a fit of the observed data to two multivariate  
 957 classifier outputs, each trained to discriminate against one of the two dominant back-  
 958 grounds of events with non-prompt leptons from  $t\bar{t}$  and of associated production of  $t\bar{t}$   
 959 and vector bosons ( $t\bar{t}W$ ,  $t\bar{t}Z$ ). The fit result is then used to set an upper limit on the  
 960 combined  $t\bar{t}H$ ,  $tHq$  and  $tHW$  production cross section, as a function of the relative  
 961 coupling strengths of Higgs and top quark and Higgs and W boson, respectively.

## 962 4.2 Data and MC Samples

963 The data considered in this analysis were collected by the CMS experiment dur-  
 964 ing 2016 and correspond to a total integrated luminosity of  $35.9\text{fb}^{-1}$ . Only periods  
 965 when the CMS magnet was on were considered when selecting the data samples, that  
 966 corresponds to the 23 Sep 2016 (Run B to G) and PromptReco (Run H) versions  
 967 of the datasets. The MC samples used in this analysis correspond to the RunI-  
 968 ISummer16MiniAODv2 campaign produced with CMSSW 80X. The two signal sam-  
 969 ples (for  $tHq$  and  $tHW$ ) were produced with MG5\_aMC@NLO (version 5.222), in  
 970 leading-order order mode, and are normalized to next-to-leading-order cross sections,  
 971 see Tab. 4.1. Each sample is generated with a set of event weights corresponding to  
 972 different values of  $\kappa_t$  and  $\kappa_V$  couplings as shown in Tab. 4.2.

### 973 4.2.1 Full 2016 dataset and MC samples

Sample	$\sigma$ [pb]	BF
/THQ_Hincl_13TeV-madgraph-pythia8_TuneCUETP8M1/	0.7927	0.324
/THW_Hincl_13TeV-madgraph-pythia8_TuneCUETP8M1/	0.1472	1.0

**Table 4.1:** Signal samples and their cross section and branching fraction used in this analysis. See Ref. [61] for more details.

974 Different MC generators were used to generate the background processes. The  
 975 dominant sources ( $t\bar{t}$ ,  $t\bar{t}W$ ,  $t\bar{t}Z$ ,  $t\bar{t}H$ ) were produced using AMC@NLO interfaced  
 976 to PYTHIA8, and are scaled to NLO cross sections. Other processes are simulated  
 977 using POWHEG interfaced to PYTHIA, or bare PYTHIA (see table 4.3 and [59]  
 978 for more details).

		<i>tHq</i>		<i>tHW</i>		
$\kappa_V$	$\kappa_t$	sum of weights	cross section [pb]	sum of weights	cross section [pb]	LHE weights
1.0	-3.0	35.700022	2.991	11.030445	0.6409	LHEweight_wgt[446]
1.0	-2.0	20.124298	1.706	5.967205	0.3458	LHEweight_wgt[447]
1.0	-1.5	14.043198	1.205	4.029093	0.2353	LHEweight_wgt[448]
1.0	-1.25	11.429338	0.9869	3.208415	0.1876	LHEweight_wgt[449]
1.0	-1.0		0.7927		0.1472	
1.0	-0.75	7.054998	0.6212	1.863811	0.1102	LHEweight_wgt[450]
1.0	-0.5	5.294518	0.4723	1.339886	0.07979	LHEweight_wgt[451]
1.0	-0.25	3.818499	0.3505	0.914880	0.05518	LHEweight_wgt[452]
1.0	0.0	2.627360	0.2482	0.588902	0.03881	LHEweight_wgt[453]
1.0	0.25	1.719841	0.1694	0.361621	0.02226	LHEweight_wgt[454]
1.0	0.5	1.097202	0.1133	0.233368	0.01444	LHEweight_wgt[455]
1.0	0.75	0.759024	0.08059	0.204034	0.01222	LHEweight_wgt[456]
1.0	1.0	0.705305	0.07096	0.273617	0.01561	LHEweight_wgt[457]
1.0	1.25	0.936047	0.0839	0.442119	0.02481	LHEweight_wgt[458]
1.0	1.5	1.451249	0.1199	0.709538	0.03935	LHEweight_wgt[459]
1.0	2.0	3.335034	0.2602	1.541132	0.08605	LHEweight_wgt[460]
1.0	3.0	10.516125	0.8210	4.391335	0.2465	LHEweight_wgt[461]
<hr/>						
1.5	-3.0	45.281492	3.845	13.426212	0.7825	LHEweight_wgt[462]
1.5	-2.0	27.606715	2.371	7.809713	0.4574	LHEweight_wgt[463]
1.5	-1.5	20.476088	1.784	5.594971	0.3290	LHEweight_wgt[464]
1.5	-1.25	17.337465	1.518	4.635978	0.2749	LHEweight_wgt[465]
1.5	-1.0	14.483302	1.287	3.775902	0.2244	LHEweight_wgt[466]
1.5	-0.75	11.913599	1.067	3.014744	0.1799	LHEweight_wgt[467]
1.5	-0.5	9.628357	0.874	2.352505	0.1410	LHEweight_wgt[468]
1.5	-0.25	7.627574	0.702	1.789184	0.1081	LHEweight_wgt[469]
1.5	0.0	5.911882	0.5577	1.324946	0.08056	LHEweight_wgt[470]
1.5	0.25	4.479390	0.4365	0.959295	0.05893	LHEweight_wgt[471]
1.5	0.5	3.331988	0.3343	0.692727	0.04277	LHEweight_wgt[472]
1.5	0.75	2.469046	0.2558	0.525078	0.03263	LHEweight_wgt[473]
1.5	1.0	1.890565	0.2003	0.456347	0.02768	LHEweight_wgt[474]
1.5	1.25	1.596544	0.1689	0.486534	0.02864	LHEweight_wgt[475]
1.5	1.5	1.586983	0.1594	0.615638	0.03509	LHEweight_wgt[476]
1.5	2.0	2.421241	0.2105	1.170602	0.06515	LHEweight_wgt[477]
1.5	3.0	7.503280	0.5889	3.467546	0.1930	LHEweight_wgt[478]
<hr/>						
0.5	-3.0	27.432685	2.260	8.929074	0.5136	LHEweight_wgt[479]
0.5	-2.0	13.956013	1.160	4.419093	0.2547	LHEweight_wgt[480]
0.5	-1.5	8.924438	0.7478	2.757611	0.1591	LHEweight_wgt[481]
0.5	-1.25	6.835341	0.5726	2.075247	0.1204	LHEweight_wgt[482]
0.5	-1.0	5.030704	0.4273	1.491801	0.08696	LHEweight_wgt[483]
0.5	-0.75	3.510528	0.2999	1.007273	0.05885	LHEweight_wgt[484]
0.5	-0.5	2.274811	0.1982	0.621663	0.03658	LHEweight_wgt[485]
0.5	-0.25	1.323555	0.1189	0.334972	0.01996	LHEweight_wgt[486]
0.5	0.0	0.656969	0.06223	0.147253	0.008986	LHEweight_wgt[487]
0.5	0.25	0.274423	0.02830	0.058342	0.003608	LHEweight_wgt[488]
0.5	0.5	0.176548	0.01778	0.068404	0.003902	LHEweight_wgt[489]
0.5	0.75	0.363132	0.03008	0.177385	0.009854	LHEweight_wgt[490]
0.5	1.0	0.834177	0.06550	0.385283	0.02145	LHEweight_wgt[491]
0.5	1.25	1.589682	0.1241	0.692099	0.03848	LHEweight_wgt[492]
0.5	1.5	2.629647	0.2047	1.097834	0.06136	LHEweight_wgt[493]
0.5	2.0	5.562958	0.4358	2.206057	0.1246	LHEweight_wgt[494]
0.5	3.0	14.843102	1.177	5.609519	0.3172	LHEweight_wgt[495]

**Table 4.2:**  $\kappa_V$  and  $\kappa_t$  combinations generated for the two signal samples and their NLO cross sections. The *tHq* cross section is multiplied by the branching fraction of the enforced leptonic decay of the top quark (0.324). See also Ref. [61].

Sample	$\sigma$ [pb]
TTWJetsToLNu_TuneCUETP8M1_13TeV-amcatnloFXFX-madspin-pythia8	0.2043
TTZToLLNuNu_M-10_TuneCUETP8M1_13TeV-amcatnlo-pythia8	0.2529
ttHJetToNonbb_M125_13TeV_amcatnloFXFX_madspin_pythia8_mWCutfix /store/cmst3/group/susy/gpetrucc/13TeV/u/TTLL_m1to10_LO_NoMS_for76X/	0.2151 0.0283
WGToLNuG_TuneCUETP8M1_13TeV-madgraphMLM-pythia8	585.8
ZGTo2LG_TuneCUETP8M1_13TeV-amcatnloFXFX-pythia8	131.3
TGJets_TuneCUETP8M1_13TeV_amcatnlo_madspin_pythia8	2.967
TGJets_TuneCUETP8M1_13TeV_amcatnlo_madspin_pythia8	2.967
TTGJets_TuneCUETP8M1_13TeV-amcatnloFXFX-madspin-pythia8	3.697
WpWpJJ_EWK-QCD_TuneCUETP8M1_13TeV-madgraph-pythia8	0.03711
ZZZ_TuneCUETP8M1_13TeV-amcatnlo-pythia8	0.01398
WWZ_TuneCUETP8M1_13TeV-amcatnlo-pythia8	0.1651
WZZ_TuneCUETP8M1_13TeV-amcatnlo-pythia8	0.05565
WW_DoubleScattering_13TeV-pythia8	1.64
tZq_ll_4f_13TeV-amcatnlo-pythia8_TuneCUETP8M1	0.0758
ST_tWll_5f_LO_13TeV-MadGraph-pythia8	0.01123
TTTT_TuneCUETP8M1_13TeV-amcatnlo-pythia8	0.009103
WZTo3LNu_TuneCUETP8M1_13TeV-powheg-pythia8	4.4296
ZZTo4L_13TeV_powheg_pythia8	1.256
TTJets_SingleLeptFromTbar_TuneCUETP8M1_13TeV-madgraphMLM-pythia8	182.1754
TTJets_SingleLeptFromT_TuneCUETP8M1_13TeV-madgraphMLM-pythia8	182.1754
TTJets_DiLept_TuneCUETP8M1_13TeV-madgraphMLM-pythia8	87.3
DYJetsToLL_M-10to50_TuneCUETP8M1_13TeV-amcatnloFXFX-pythia8	18610
DYJetsToLL_M-50_TuneCUETP8M1_13TeV-madgraphMLM-pythia8	6024
WJetsToLNu_TuneCUETP8M1_13TeV-amcatnloFXFX-pythia8	61526.7
ST_tW_top_5f_inclusiveDecays_13TeV-powheg-pythia8_TuneCUETP8M1	35.6
ST_tW_antitop_5f_inclusiveDecays_13TeV-powheg-pythia8_TuneCUETP8M1	35.6
ST_t-channel_4f_leptonDecays_13TeV-amcatnlo-pythia8_TuneCUETP8M1	70.3144
ST_t-channel_antitop_4f_leptonDecays_13TeV-powheg-pythia8_TuneCUETP8M1	26.2278
ST_s-channel_4f_leptonDecays_13TeV-amcatnlo-pythia8_TuneCUETP8M1	3.68064
WWTo2L2Nu_13TeV-powheg	10.481

**Table 4.3:** List of background samples used in this analysis (CMSSW 80X). In the first section of the table are listed the samples of the processes for which we use the simulation to extract the final yields and shapes, in the second section the samples of the processes we will estimate from data. The MC simulation is used to design the data driven methods and derive the associated systematics.

Sample	$\sigma$ [pb]
ttWJets_13TeV_madgraphMLM	0.6105
ttZJets_13TeV_madgraphMLM	0.5297/0.692

**Table 4.4:** Leading-order  $t\bar{t}W$  and  $t\bar{t}Z$  samples used in the signal BDT training.

Three lepton and Four lepton
HLT_DiMu9_Ele9_CaloIdL_TrackIdL_v*
HLT_Mu8_DiEle12_CaloIdL_TrackIdL_v*
HLT_TripleMu_12_10_5_v*
HLT_Ele16_Ele12_Ele8_CaloIdL_TrackIdL_v*
HLT_Mu23_TrkIsoVVL_Ele8_CaloIdL_TrackIdL_IsoVL_v*
HLT_Mu23_TrkIsoVVL_Ele8_CaloIdL_TrackIdL_IsoVL_DZ_v*
HLT_Mu8_TrkIsoVVL_Ele23_CaloIdL_TrackIdL_IsoVL_v*
HLT_Mu8_TrkIsoVVL_Ele23_CaloIdL_TrackIdL_IsoVL_DZ_v*
HLT_Ele23_Ele12_CaloIdL_TrackIdL_IsoVL_DZ_v*
HLT_Mu17_TrkIsoVVL_Mu8_TrkIsoVVL_DZ_v*
HLT_Mu17_TrkIsoVVL_TkMu8_TrkIsoVVL_DZ_v*
HLT_IsoMu22_v*
HLT_IsoTkMu22_v*
HLT_IsoMu22_eta2p1_v*
HLT_IsoTkMu22_eta2p1_v*
HLT_IsoMu24_v*
HLT_IsoTkMu24_v*
HLT_Ele27_WPTight_Gsf_v*
HLT_Ele25_eta2p1_WPTight_Gsf_v*
HLT_Ele27_eta2p1_WPLoose_Gsf_v*

**Table 4.5:** Table of high-level triggers that we consider in the analysis.

### 979 4.2.2 Triggers

980 We consider online-reconstructed events triggered by one, two, or three leptons.  
 981 Single-lepton triggers are included to boost the acceptance of events where the  $p_T$  of  
 982 the sub-leading lepton falls below the threshold of the double-lepton triggers. Ad-  
 983 ditionally, by including double-lepton triggers in the  $\geq 3$  lepton category, as well  
 984 as single-lepton triggers in all categories, we increase the efficiency, considering the  
 985 logical “or” of the trigger decisions of all the individual triggers in a given category.  
 986 Tab. 4.5 shows the lowest-threshold non-prescaled triggers present in the High-Level  
 987 Trigger (HLT) menus for both Monte-Carlo and data in 2016.

#### 988 4.2.2.1 Trigger efficiency scale factors

989 The efficiency of events to pass the trigger is measured in simulation (trivially using  
 990 generator information) and in the data (using event collected by an uncorrelated

Category	Scale Factor
ee	$1.01 \pm 0.02$
e $\mu$	$1.01 \pm 0.01$
$\mu\mu$	$1.00 \pm 0.01$
3l	$1.00 \pm 0.03$

**Table 4.6:** Trigger efficiency scale factors and associated uncertainties, shown here rounded to the nearest percent.

991 MET trigger). Small differences between the data and MC efficiencies are corrected  
 992 by applying scale factors as shown in Tab. 4.6. The exact procedure and control plots  
 993 are documented in [62] for the current analysis.

## 994 4.3 Object Identification and event selection

### 995 4.3.1 Jets and $b$ tagging

996 The analysis uses anti- $k_t$  (0.4) particle-flow (PF) jets, corrected for charged hadrons  
 997 not coming from the primary vertex (charged hadron subtraction), and having jet  
 998 energy corrections (`Summer16_23Sep2016V3`) applied as a function of the jet  $E_T$  and  
 999  $\eta$ . Jets are only considered if they have a transverse energy above 25GeV.

1000 In addition, they are required to be separated from any lepton candidates passing  
 1001 the fakeable object selections (see Tables 4.7 and 4.8) by  $\Delta R > 0.4$ .

1002 The loose and medium working points of the CSV b-tagging algorithm are used to  
 1003 identify  $b$  jets. Data/simulation differences in the  $b$  tagging performance are corrected  
 1004 by applying per-jet weights to the simulation, dependent on the jet  $p_T$ , eta,  $b$  tagging  
 1005 discriminator, and flavor (from simulation truth) [63]. The per-event weight is taken  
 1006 as the product of the per-jet weights, including those of the jets associated to the  
 1007 leptons. More details can be found in the corresponding  $t\bar{t}H$  documentation [59, 62].

1008 **4.3.2 Lepton selection**

Cut	Loose	Fakeable object	Tight
$ \eta  < 2.4$	✓	✓	✓
$p_T$	$> 5\text{GeV}$	$> 15\text{GeV}$	$> 15\text{GeV}$
$ d_{xy}  < 0.05 \text{ (cm)}$	✓	✓	✓
$ d_z  < 0.1 \text{ (cm)}$	✓	✓	✓
$\text{SIP}_{3D} < 8$	✓	✓	✓
$I_{\text{mini}} < 0.4$	✓	✓	✓
is Loose Muon	✓	✓	✓
jet CSV	—	$< 0.8484$	$< 0.8484$
is Medium Muon	—	—	✓
tight-charge	—	—	✓
lepMVA $> 0.90$	—	—	✓

**Table 4.7:** Requirements on each of the three muon selections. In the cases where the cut values change between the selections, those values are listed in the table. Otherwise, whether the cut is applied is indicated. For the two  $p_T^{\text{ratio}}$  and CSV rows, the cuts marked with a † are applied to leptons that fail the lepton MVA cut, while the loose cut value is applied to those that pass the lepton MVA cut.

1009       The lepton reconstruction and selection is identical to that used in the  $t\bar{t}H$  mul-  
 1010 tilepton analysis, as documented in Refs. [59, 62]. For details on the reconstruction  
 1011 algorithms, isolation, pileup mitigation, and a description of the lepton MVA discrim-  
 1012 inator and validation plots thereof, we refer to that document since they are out of  
 1013 the scope of this thesis. Three different selections are defined both for the electron  
 1014 and muon object identification: the *Loose*, *Fakeable Object*, and *Tight* selection. As  
 1015 described in more detail later, these are used for event level vetoes, the fake rate  
 1016 estimation application region, and the final signal selection, respectively. The  $p_T$  of  
 1017 fakeable objects is defined as  $0.85 \times p_T(\text{jet})$ , where the jet is the one associated to the  
 1018 lepton object. This mitigates the dependence of the fake rate on the momentum of  
 1019 the fakeable object and thereby improves the precision of the method.

1020       Tables 4.7 and 4.8 list the full criteria for the different selections of muons and  
 1021 electrons.

Cut	Loose	Fakeable Object	Tight
$ \eta  < 2.5$	✓	✓	✓
$p_T$	$> 7\text{GeV}$	$> 15\text{GeV}$	$> 15\text{GeV}$
$ d_{xy}  < 0.05 \text{ (cm)}$	✓	✓	✓
$ d_z  < 0.1 \text{ (cm)}$	✓	✓	✓
$\text{SIP}_{3D} < 8$	✓	✓	✓
$I_{\text{mini}} < 0.4$	✓	✓	✓
MVA ID $> (0.0, 0.0, 0.7)$	✓	✓	✓
$\sigma_{i\eta i\eta} < (0.011, 0.011, 0.030)$	—	✓	✓
$\text{H/E} < (0.10, 0.10, 0.07)$	—	✓	✓
$\Delta\eta_{in} < (0.01, 0.01, 0.008)$	—	✓	✓
$\Delta\phi_{in} < (0.04, 0.04, 0.07)$	—	✓	✓
$-0.05 < 1/E - 1/p < (0.010, 0.010, 0.005)$	—	✓	✓
$p_T^{\text{ratio}}$	—	$> 0.5 \dagger / -$	—
jet CSV	—	$< 0.3 \dagger / < 0.8484$	$< 0.8484$
tight-charge	—	—	✓
conversion rejection	—	—	✓
Number of missing hits	$< 2$	$== 0$	$== 0$
lepMVA $> 0.90$	—	—	✓

**Table 4.8:** Criteria for each of the three electron selections. In cases where the cut values change between selections, those values are listed in the table. Otherwise, whether the cut is applied is indicated. In some cases, the cut values change for different  $\eta$  ranges. These ranges are  $0 < |\eta| < 0.8$ ,  $0.8 < |\eta| < 1.479$ , and  $1.479 < |\eta| < 2.5$  and the respective cut values are given in the form (value<sub>1</sub>, value<sub>2</sub>, value<sub>3</sub>).

### 4.3.3 Lepton selection efficiency

Efficiencies of reconstruction and selecting loose leptons are measured both for muons and electrons using a tag and probe method on both data and MC, using  $Z \rightarrow \ell^+\ell^-$ . Corresponding scale factors are derived from the ratio of efficiencies and applied to the selected These. Events are produced for the leptonic SUSY analyses using equivalent lepton selections and recycled for the  $t\bar{t}H$  analysis as well as for this analysis. The efficiencies of applying the tight selection as defined in Tables 4.7 and 4.8, on the loose leptons are determined again by using a tag and probe method on a sample of DY-enriched events. They are documented for the  $t\bar{t}H$  analysis in Ref. [62] and are exactly equivalent for this analysis.

## 1032 4.4 Background predictions

1033 The modeling of reducible and irreducible backgrounds in this analysis uses the exact  
 1034 methods, analysis code, and ROOT trees used for the  $t\bar{t}H$  multilepton analysis. We  
 1035 give a brief description of the methods and refer to the documentation of that analysis  
 1036 in Refs. [59, 62] for any details.

1037 The backgrounds in three-lepton final states can be split in two broad categories:  
 1038 irreducible backgrounds with genuine prompt leptons (i.e. from on-shell W and Z  
 1039 boson decays); and reducible backgrounds where at least one of the leptons is “non-  
 1040 prompt”, i.e. produced within a hadronic jet, either a genuine lepton from heavy  
 1041 flavor decays, or simply mis-reconstructed jets.

1042 Irreducible backgrounds can be reliably estimated directly from Monte-Carlo sim-  
 1043 ulated events, using higher-order cross sections or data control regions for the overall  
 1044 normalization. This is done in this analysis for all backgrounds involving prompt lep-  
 1045 tons:  $t\bar{t}W$ ,  $t\bar{t}Z$ ,  $t\bar{t}H$ ,  $WZ$ ,  $ZZ$ ,  $W^\pm W^\pm qq$ ,  $t\bar{t}t\bar{t}$ ,  $tZq$ ,  $tZW$ ,  $WWW$ ,  $WWZ$ ,  $WZZ$ ,  
 1046  $ZZZ$ .

1047 Reducible backgrounds, on the other hand, are not well predicted by simulation,  
 1048 and are estimated using data-driven methods. In the case of non-prompt leptons, a  
 1049 fake rate method is used, where the contribution to the final selection is estimated by  
 1050 extrapolating from a sideband (or “application region”) with a looser lepton definition  
 1051 (the fakeable object definitions in Tabs. 4.7 and 4.8) to the signal selection. The tight-  
 1052 to-loose ratios (or “fake rates”) are measured in several background dominated data  
 1053 events with dedicated triggers, subtracting the residual prompt lepton contribution  
 1054 using MC. Non-prompt leptons in our signal regions are predominantly produced in  $t\bar{t}$   
 1055 events, with a much smaller contribution, from Drell–Yan production. The systematic  
 1056 uncertainty on the normalization of the non-prompt background estimation is on the

order of 50%, and thereby one of the dominant limitations on the performance of multilepton analyses in general and this analysis in particular. It consists of several individual sources, such as the result of closure tests of the method using simulated events, limited statistics in the data control regions due to necessary prescaling of lepton triggers, and the uncertainty in the subtraction of residual prompt leptons from the control region.

The fake background where the leptons pass the looser selection are weighted according to how many of them fail the tight criteria. Events with a single failing lepton are weighted with the factor  $f/(1-f)$  for the estimate to the tight selection region, where  $f$  is the fake rate. Events with two failing leptons are given the negative weight  $-f_i f_j / (1-f_i)(1-f_j)$ , and for three leptons the weight is positive and equal to the product of  $f/(1-f)$  factor evaluated for each failing lepton.

Figures 4.2 show the distributions of some relevant kinematic variables, normalized to the cross section of the respective processes and to the integrated luminosity.

## 4.5 Signal discrimination

The  $tHq$  signal is separated from the main backgrounds using a boosted decision tree (BDT) classifier, trained on simulated signal and background events. A set of discriminating variables are given as input to the BDT which produces a output distribution maximizing the discrimination power. Table 4.9 lists the input variables used while Figures 4.3 show their distributions for the relevant signal and background samples, for the three lepton channel. Two BDT classifiers are trained for the two main backgrounds expected in the analysis: events with prompt leptons from  $t\bar{t}W$  and  $t\bar{t}Z$ (also referred to as  $t\bar{t}V$ ), and events with non-prompt leptons from  $t\bar{t}$ . The datasets used in the training are the  $tHq$  signal (see Tab. 4.1), and LO MADGRAPH samples

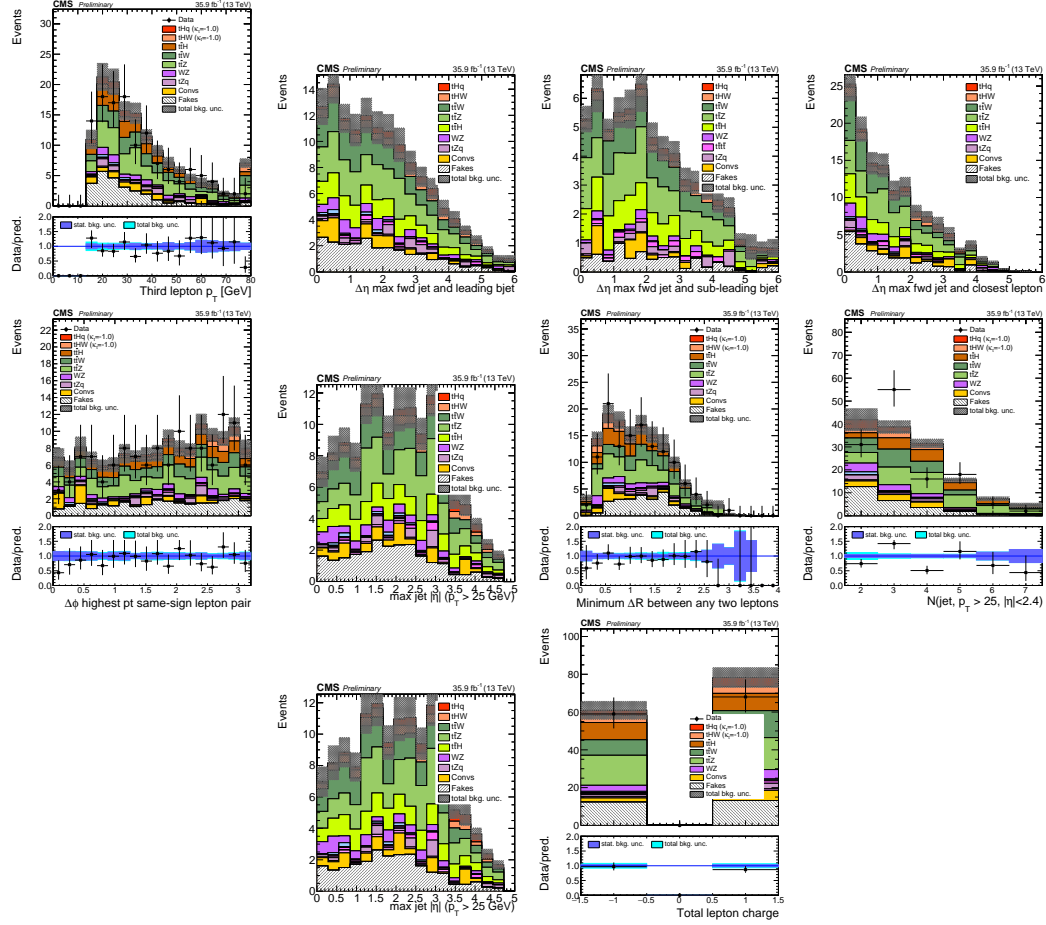


**Figure 4.2:** Distributions of input variables to the BDT for signal discrimination, three lepton channel, normalized to their cross section and to  $35.9\text{fb}^{-1}$ .

of  $t\bar{t}W$  and  $t\bar{t}Z$ , in an admixture proportional to their respective cross sections (see Tab. 4.4).

The MVA analysis consist of two stages: first a “training” where the MVA method is trained to discriminate between simulated signal and background events, then a “test” stage where the trained algorithm is used to classify different events from the samples. The sample is obtained from a pre-selection (see Tab. ?? with pre-selection cuts). Figures 4.4 show the input variables distributions as seen by the MVA algorithm. Note that in contrast to the distributions in Fig. 4.3 only the main backgrounds ( $t\bar{t}$  from simulation,  $t\bar{t}V$ ) are included.

Variable name	Description
nJet25	Number of jets with $p_T > 25$ GeV, $ \eta  < 2.4$
MaxEtaJet25	Maximum $ \eta $ of any (non-CSV-loose) jet with $p_T > 25$ GeV
totCharge	Sum of lepton charges
nJetEta1	Number of jets with $ \eta  > 1.0$ , non-CSV-loose
detaFwdJetBJet	$\Delta\eta$ between forward light jet and hardest CSV loose jet
detaFwdJet2BJet	$\Delta\eta$ between forward light jet and second hardest CSV loose jet (defaults to -1 in events with only one CSV loose jet)
detaFwdJetClosestLep	$\Delta\eta$ between forward light jet and closest lepton
dphiHighestPtSSPair	$\Delta\phi$ of highest $p_T$ same-sign lepton pair
minDRll	minimum $\Delta R$ between any two leptons
Lep3Pt/Lep2Pt	$p_T$ of the 3 <sup>rd</sup> lepton (2 <sup>nd</sup> for ss2l)

**Table 4.9:** MVA input discriminating variables

1090 Note that splitting the training in two groups reveals that some variables show  
 1091 opposite behavior for the two background sources; potentially screening the discrimi-  
 1092 nation power if they were to be used in a single discriminant. For some other variables  
 1093 the distributions are similar in both background cases.

1094 From table 4.9, it is clear that the input variables are correlated to some extend.  
 1095 These correlations play an important role for some MVA methods like the Fisher  
 1096 discriminant method in which the first step consist of performing a linear transfor-  
 1097 mation to an phase space where the correlations between variables are removed. In  
 1098 case a boosted decision tree (BDT) method however, correlations do not affect the  
 1099 performance. Figure 4.6 show the linear correlation coefficients for signal and back-  
 1100 ground for the two training cases (the signal values are identical by construction). As  
 1101 expected, strong correlations appears for variables related to the forward jet activity.  
 1102 Same trend is seen in case of the same sign dilepton channel in Figure ??.

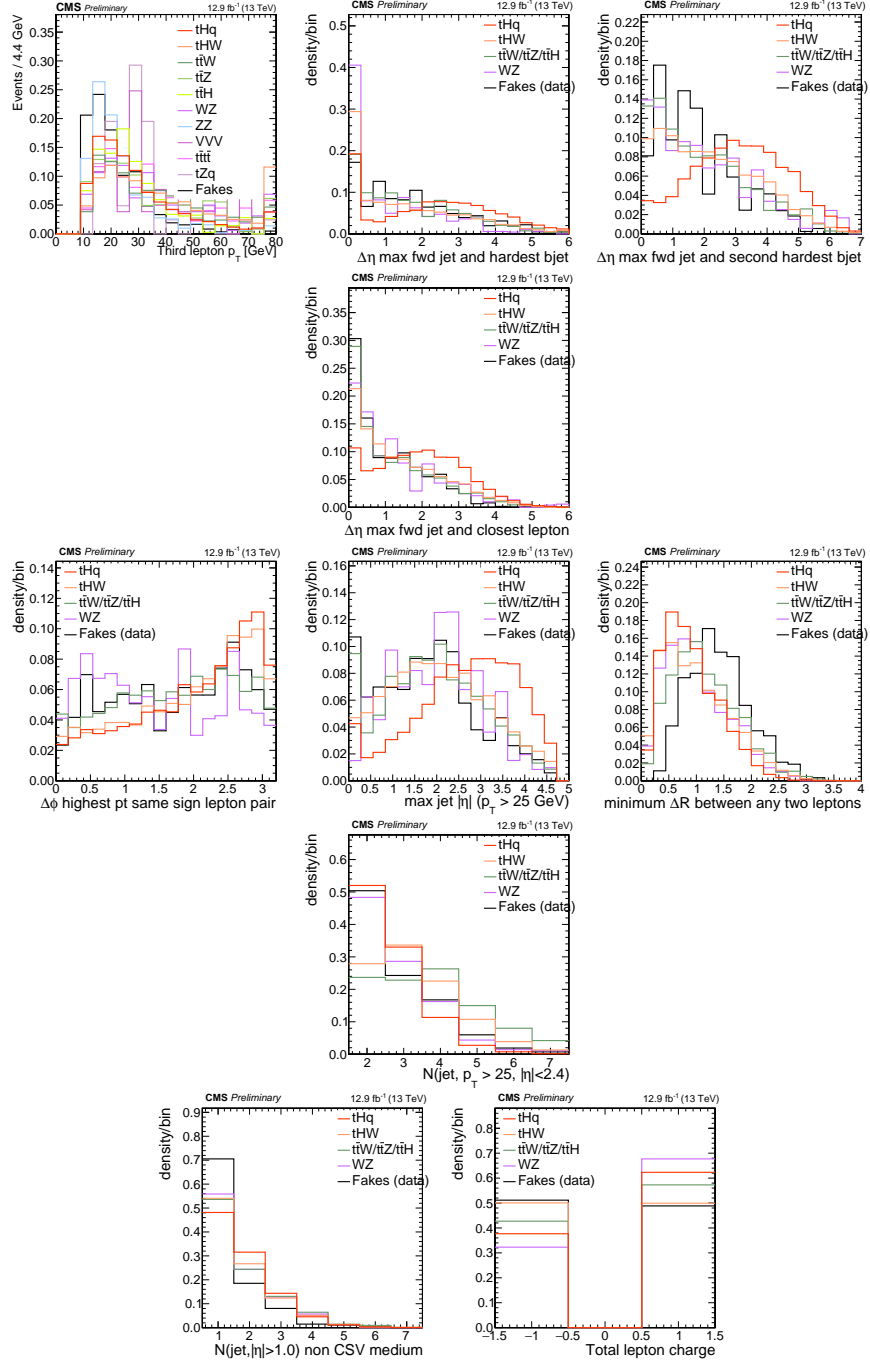


**Figure 4.3:** Distributions of input variables to the BDT for signal discrimination, three lepton channel.

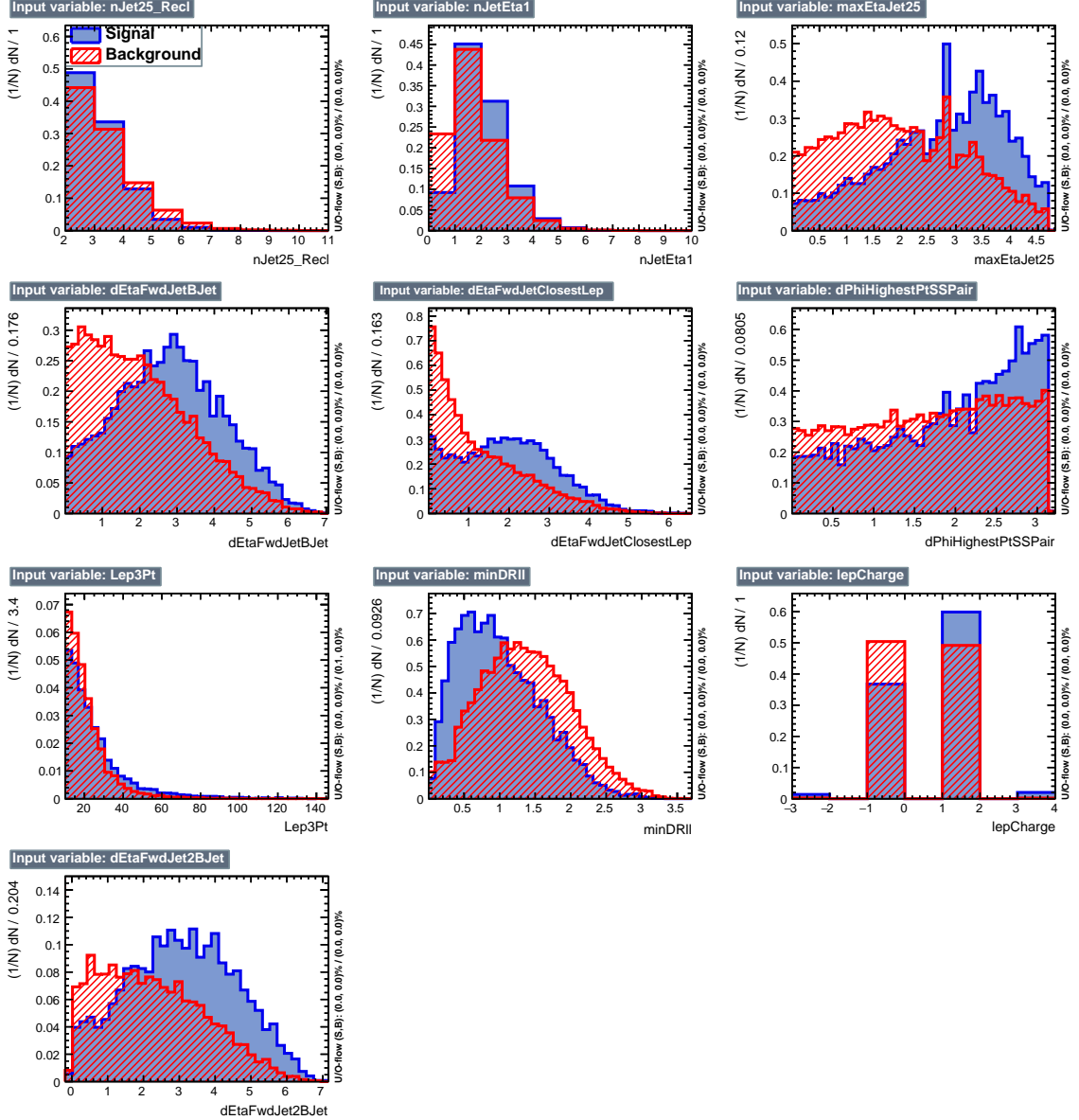


**Figure 4.4:** BDT inputs as seen by TMVA (signal, in blue, is  $tHq$ , background, in red, is  $t\bar{t}$ ) for the three lepton channel, discriminated against  $t\bar{t}$  (fakes) background.

### 1103 4.5.1 Classifiers response

1104 Several MVA algorithms were evaluated to determine the most appropriate method  
 1105 for this analysis. The plots in Fig. 4.7 (top) show the background rejection as a  
 1106 function of the signal efficiency for  $t\bar{t}$  and  $t\bar{t}V$  trainings (ROC curves) for the different

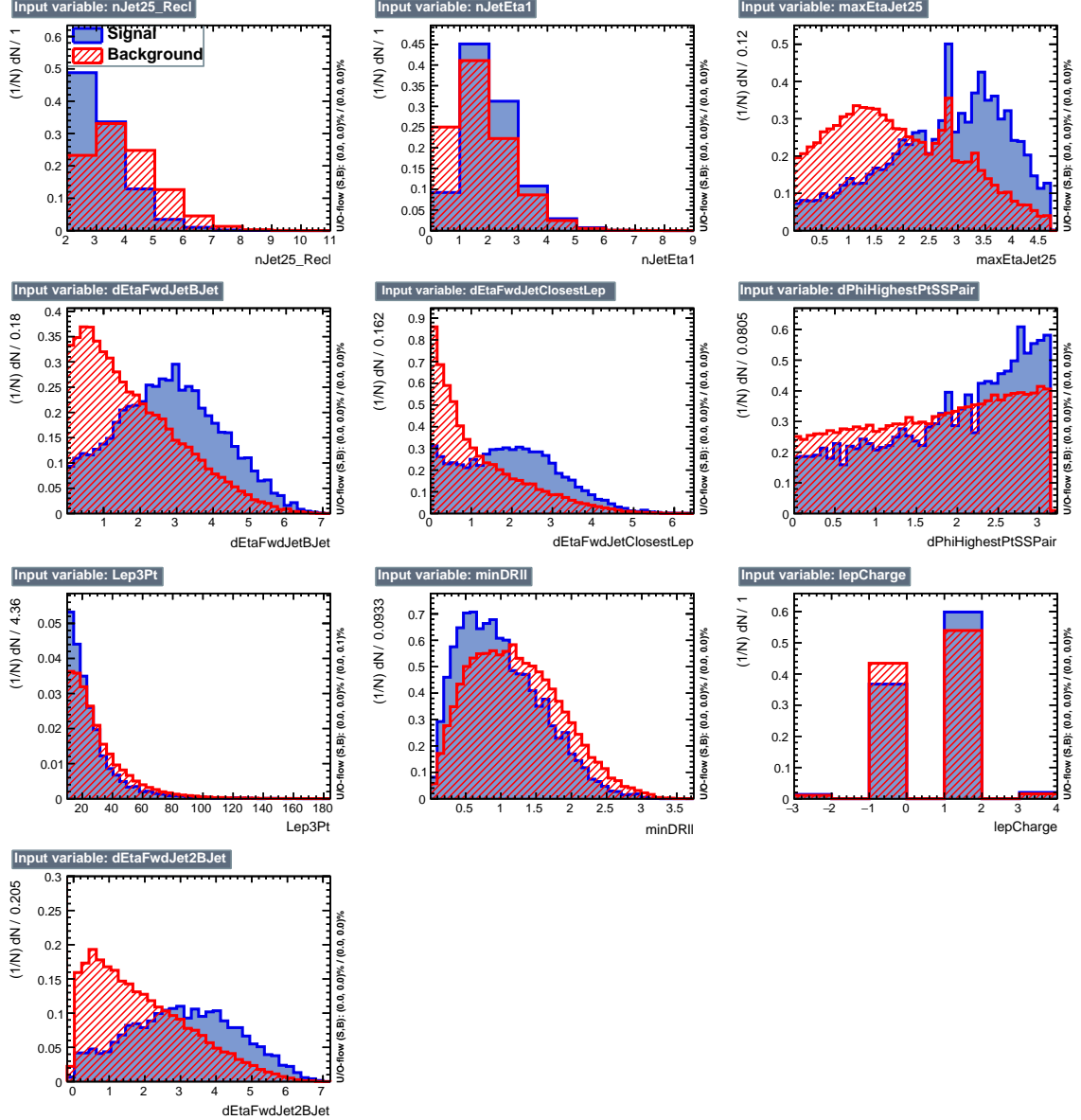


**Figure 4.5:** BDT inputs as seen by TMVA (signal, in blue, is  $tHq$ , background, in red, is  $t\bar{t}W+t\bar{t}Z$ ) for the three lepton channel, discriminated against  $t\bar{t}V$  background.

algorithms that were evaluated.

In both cases the gradient boosted decision tree (“BDTA\_GRAD”) classifier offers the best results, followed by an adaptive BDT classifier (“BDTA”). The BDTA\_GRAD classifier output distributions for signal and backgrounds are shown on the bottom of Fig. 4.7. As expected, a good discrimination power is obtained using default discrim-

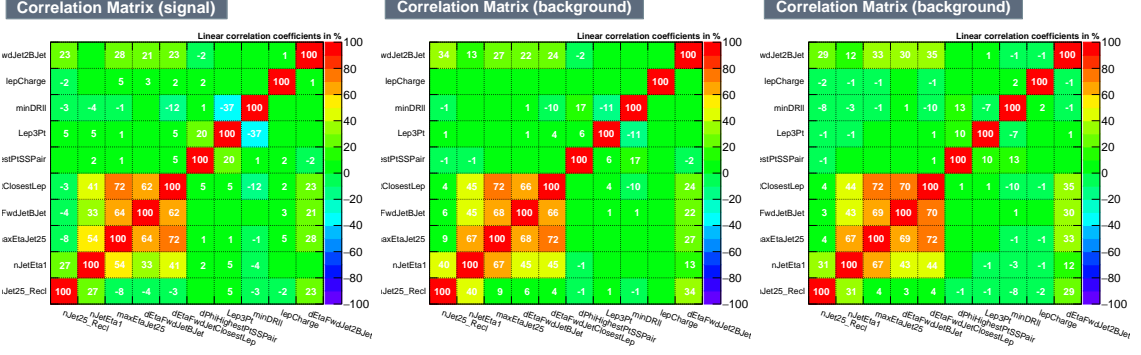


**Figure 4.6:** Signal (left),  $t\bar{t}$  background (middle), and  $t\bar{t}V$  background (right.) correlation matrices for the input variables in the TMVA analysis for the three lepton channel.

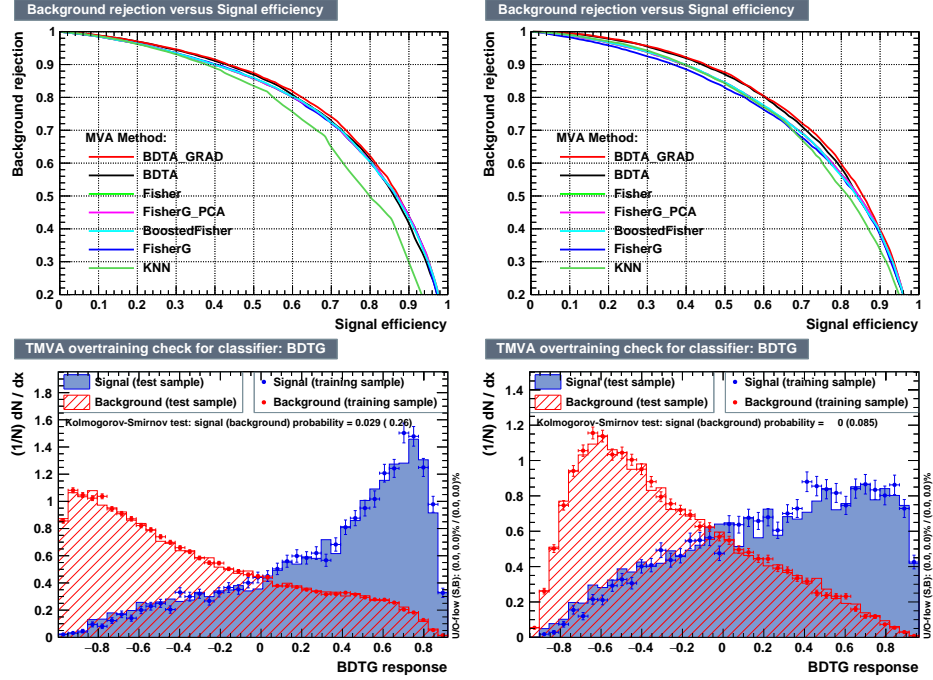


**Figure 4.7:** Top: background rejection vs signal efficiency (ROC curves) for various MVA classifiers (top) in the three lepton channel against  $t\bar{t}V$  (left) and  $t\bar{t}$  (right). Bottom: classifier output distributions for the gradient boosted decision trees, for training against  $t\bar{t}V$  (left) and against  $t\bar{t}$  (right).

inator parameter values, with minimal overtraining. TMVA provides a ranking of the  
1113 input variables by their importance in the classification process, shown in Tab. 4.10.  
1114 The TMVA settings used in the BDT training are shown in Tab. 4.11.

ttbar training			ttV training		
Rank	Variable	Importance	Variable	Importance	Importance
1	minDRll	1.329e-01	dEtaFwdJetBJet	1.264e-01	
2	dEtaFwdJetClosestLep	1.294e-01	Lep3Pt	1.224e-01	
3	dEtaFwdJetBJet	1.209e-01	maxEtaJet25	1.221e-01	
4	dPhiHighestPtSSPair	1.192e-01	dEtaFwdJet2BJet	1.204e-01	
5	Lep3Pt	1.158e-01	dEtaFwdJetClosestLep	1.177e-01	
6	maxEtaJet25	1.121e-01	minDRll	1.143e-01	
7	dEtaFwdJet2BJet	9.363e-02	dPhiHighestPtSSPair	9.777e-02	
8	nJetEta1	6.730e-02	nJet25_Recl	9.034e-02	
9	nJet25_Recl	6.178e-02	nJetEta1	4.749e-02	
10	lepCharge	4.701e-02	lepCharge	4.116e-02	

**Table 4.10:** TMVA input variables ranking for BDTA\_GRAD method for the trainings in the three lepton channel. For both trainings the rankings show almost the same 5 variables in the first places.

---

```
TMVA.Types.kBDT
NTrees=800
BoostType=Grad
Shrinkage=0.10
!UseBaggedGrad
nCuts=50
MaxDepth=3
NegWeightTreatment=PairNegWeightsGlobal
CreateMVApdfs
```

---

**Table 4.11:** TMVA configuration used in the BDT training.

## 1115 4.6 Additional discriminating variables

1116 Two additional discriminating variables were tested considering the fact that the  
 1117 forward jet in the background could come from the pileup; since we have a real  
 1118 forward jet in the signal, it could give some improvement in the discriminating power.  
 1119 The additional variables describe the forward jet momentum (fwdJetPt25) and the  
 1120 forward jet identification(fwdJetPUID). Distributions for these variables in the three  
 1121 lepton channel are shown in the figure 4.8. The forward jet identification distribution  
 1122 show that for both, signal and background, jets are mostly real jets.

1123 The testing was made including in the MVA input one variable at a time, so we

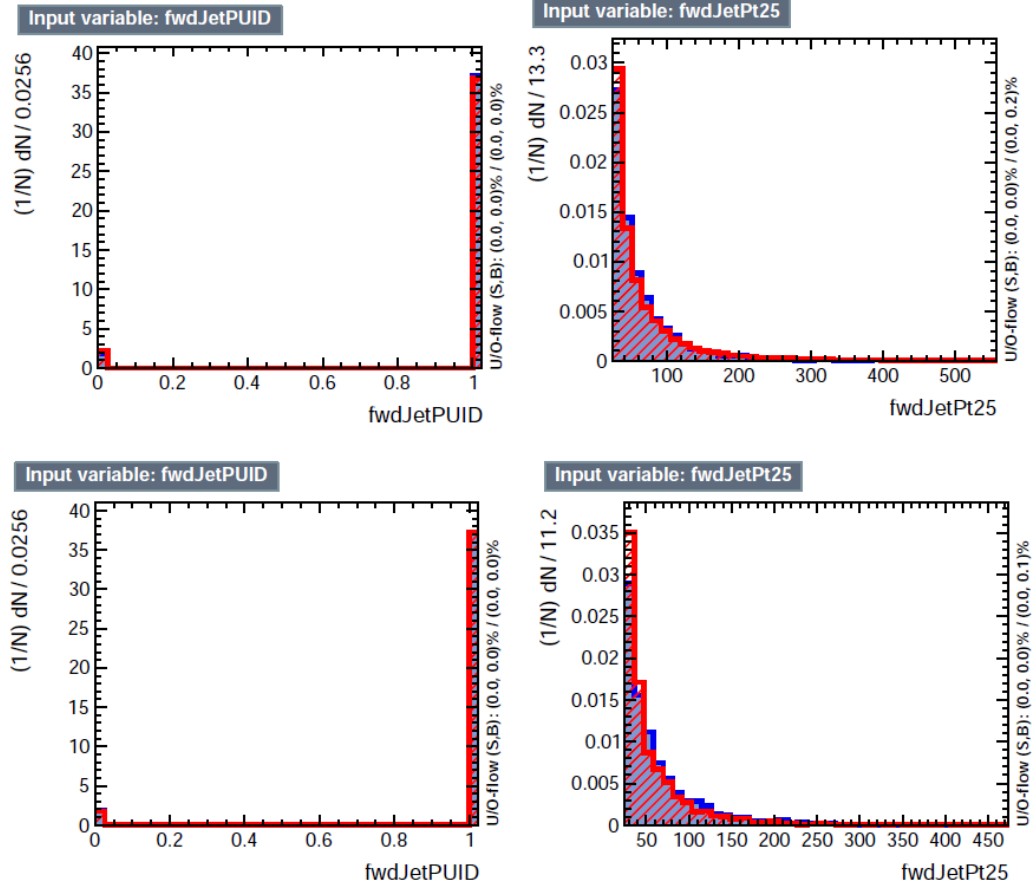


**Figure 4.8:** Additional discriminating variables distributions for ttV training (Top row) and tt training (bottom row) in the three lepton channel. The origin of the jets in the forward jet identification distribution is tagged as 0 for “pileup jets” while “real jets” are tagged as 1.

can evaluate the discrimination power of each variable, and then both simultaneously. fwdJetPUID was ranked in the last place in importance (11) in both training (ttV and tt) while fwdJetPt25 was ranked 3 in the ttV training and 7 in the tt training. When training using 12 variables, fwdJetPt25 was ranked 5 and 7 in the ttV and tt trainings respectively, while fwdJetPUID was ranked 12 in both cases.

The improvement in the discrimination performance provided by the additional variables is about 1%, so it was decided not to include them in the procedure. Table 4.12 show the ROC-integral for all the testing cases we made.

ROC-integral	
base 10 var ttv	0.848
+ fwdJetPUID ttv	0.849
+ fwdJetPt25 ttv	0.856
12 var ttv	0.856
<hr/>	
base 10 var tt	0.777
+ fwdJetPUID tt	0.777
+ fwdJetPt25 tt	0.787
12 var	0.787

**Table 4.12:** ROC-integral for all the testing cases we made in the evaluation of the additional variables discriminating power. The improvement in the discrimination performance provided by the additional variables is about 1%

<sup>1132</sup> **Chapter 5**

<sup>1133</sup> **The CMS forward pixel detector**

<sup>1134</sup> **5.0.1 The phase 1 FPix upgrade**

<sup>1135</sup> **5.0.2 FPix module production line**

<sup>1136</sup> **5.0.3 The Gluing stage**

<sup>1137</sup> **5.0.4 The Encapsulation stage**

<sup>1138</sup> **5.0.5 The FPix module production yields**

# <sup>1139</sup> References

- <sup>1140</sup> [1] D.J. Griffiths, “Introduction to electrodynamics”. 4th ed. Pearson, (2013).
- <sup>1141</sup> [2] F. Mandl, G. Shaw. “Quantum field theory.” Chichester: Wiley (2009).
- <sup>1142</sup> [3] F. Halzen, and A.D. Martin, “Quarks and leptons: An introductory course in  
<sup>1143</sup> modern particle physics”. New York: Wiley, (1984) .
- <sup>1144</sup> [4] J.C. Maxwell. “A dynamical theory of the electromagnetic field”. Philosophical Transactions of the Royal Society of London. 155: 459–512.(1865)  
<sup>1145</sup>  
<sup>1146</sup> doi:10.1098/rstl.1865.0008
- <sup>1147</sup> [5] M. Planck. “Über das Gesetz der Energieverteilung im Normalspektrum”.  
<sup>1148</sup> Annalen der Physik. 4 (3): 553.(1901).
- <sup>1149</sup> [6] A. Einstein “Über einen die Erzeugung und Verwandlung des Lichtes betref-  
<sup>1150</sup> fenden heuristischen Gesichtspunkt”. Annalen der Physik. 17 (6): 132–148,  
<sup>1151</sup> (1905).
- <sup>1152</sup> [7] A. Einstein. “Über die von der molekularkinetischen Theorie der Wärme  
<sup>1153</sup> geforderte Bewegung von in ruhenden Flüssigkeiten suspendierten Teilchen”.  
<sup>1154</sup> Annalen der Physik. 17 (8): 549–560, (1905).
- <sup>1155</sup> [8] A. Einstein. “Zur Elektrodynamik bewegter Körper”. Annalen der Physik. 17  
<sup>1156</sup> (10): 891–921, (1905).

- 1157 [9] A. Einstein, "Ist die TrÄdgheit eines KÃürpers von seinem Energieinhalt ab-  
 1158 hÃdngig?". Annalen der Physik. 18 (13): 639â€¢641, (1905).
- 1159 [10] B. P. Abbott et al. "Observation of Gravitational Waves from a Binary Black  
 1160 Hole Merger". PRL 116, 061102 (2016).
- 1161 [11] J. Schwinger. "Quantum Electrodynamics. I. A Covariant Formulation". Phys-  
 1162 ical Review. 74 (10): 1439â€¢61, (1948).
- 1163 [12] R. P. Feynman. "Spaceâ€¢Time Approach to Quantum Electrodynamics".  
 1164 Physical Review. 76 (6): 769â€¢89, (1949).
- 1165 [13] S. Tomonaga. "On a Relativistically Invariant Formulation of the Quantum  
 1166 Theory of Wave Fields". Progress of Theoretical Physics. 1 (2): 27â€¢42, (1946).
- 1167 [14] S.L. Glashow. "Partial symmetries of weak interactions", Nucl. Phys. 22 579-  
 1168 588, (1961).
- 1169 [15] A. Salam, J.C. Ward. "Electromagnetic and weak interactions", Physics Letters  
 1170 13 168-171, (1964).
- 1171 [16] S. Weinberg, "A model of leptons", Physical Review Letters, vol. 19, no. 21, p.  
 1172 1264, (1967).
- 1173 [17] E. Noether, "Invariante Variationsprobleme", Nachrichten von der Gesellschaft  
 1174 der Wissenschaften zu GÃüttingen, mathematisch-physikalische Klasse, vol.  
 1175 1918, pp. 235â€¢257, (1918).
- 1176 [18] File:Standard\_Model\_of\_Elementary\_Particle\_dark.svg. (2017, June 12)  
 1177 Wikimedia Commons, the free media repository. Retrieved November 27,  
 1178 2017 from <https://www.collegiate-advanced-electricity.com/single-post/2017/04/10/The-Standard-Model-of-Particle-Physics>.

- 1180 [19] M. Goldhaber, L. Grodzins, A.W. Sunyar “Helicity of Neutrinos”, Phys. Rev.  
 1181 109, 1015 (1958).
- 1182 [20] Palanque-Delabrouille N et al. “Neutrino masses and cosmology with Lyman-  
 1183 alpha forest power spectrum”, JCAP 11 011 (2015).
- 1184 [21] C. Patrignani et al. (Particle Data Group), Chin. Phys. C, 40, 100001 (2016)  
 1185 and 2017 update.
- 1186 [22] M. Gell-Mann. “A Schematic Model of Baryons and Mesons”. Physics Letters.  
 1187 8 (3): 214–215 (1964).
- 1188 [23] G. Zweig. “An SU(3) Model for Strong Interaction Symmetry and its Breaking”  
 1189 (PDF). CERN Report No.8182/TH.401 (1964).
- 1190 [24] G. Zweig. “An SU(3) Model for Strong Interaction Symmetry and its Breaking:  
 1191 II” (PDF). CERN Report No.8419/TH.412(1964).
- 1192 [25] M. Gell-Mann. “The Interpretation of the New Particles as Displaced Charged  
 1193 Multiplets”. Il Nuovo Cimento 4: 848. (1956).
- 1194 [26] T. Nakano, K. Nishijima. “Charge Independence for V-particles”. Progress of  
 1195 Theoretical Physics 10 (5): 581-582. (1953).
- 1196 [27] N. Cabibbo, “Unitary symmetry and leptonic decays” Physical Review Letters,  
 1197 vol. 10, no. 12, p. 531, (1963).
- 1198 [28] M.Kobayashi, T.Maskawa, “CP-violation in the renormalizable theory of weak  
 1199 interaction,” Progress of Theoretical Physics, vol. 49, no. 2, pp. 652-657, (1973).
- 1200 [29] File:Weak Decay (flipped).svg. (2017, June 12). Wikimedia Commons,  
 1201 the free media repository. Retrieved November 27, 2017

- 1202       from     `https : //commons.wikimedia.org/w/index.php?title = File :`  
 1203       `Weak_Decay_(flipped).svg&oldid = 247498592.`
- 1204 [30] Georgia Tech University. Coupling Constants for the Fundamental  
 1205 Forces(2005). Retrieved January 10, 2018, from `http://hyperphysics.phy –`  
 1206 `astr.gsu.edu/hbase/Forces/couple.html#c2`
- 1207 [31] M. Strassler. (May 31, 2013).The Strengths of the Known Forces. Retrieved  
 1208 January 10, 2018, from `https://profmattstrassler.com/articles – and –`  
 1209 `posts/particle – physics – basics/the – known – forces – of – nature/the –`  
 1210 `strength – of – the – known – forces/`
- 1211 [32] M. Peskin, D. Schroeder, “An introduction to quantum field theory”. Perseus  
 1212 Books Publishing L.L.C., (1995).
- 1213 [33] A. Pich. “The Standard Model of Electroweak Interactions”  
 1214 `https://arxiv.org/abs/1201.0537`
- 1215 [34] F.Bellaiche. (2012, 2 September). “What’s this Higgs boson anyway?”. Retrieved  
 1216 from: `https://www.quantum-bits.org/?p=233`
- 1217 [35] M. Endres et al. Nature 487, 454-458 (2012) doi:10.1038/nature11255
- 1218 [36] F. Englert, R. Brout. “Broken Symmetry and the Mass of Gauge Vec-  
 1219 tor Mesons”. Physical Review Letters. 13 (9): 321–323.(1964) Bib-  
 1220 code:1964PhRvL..13..321E. doi:10.1103/PhysRevLett.13.321
- 1221 [37] P.Higgs. “Broken Symmetries and the Masses of Gauge Bosons”. Physical  
 1222 Review Letters. 13 (16): 508–509,(1964). Bibcode:1964PhRvL..13..508H.  
 1223 doi:10.1103/PhysRevLett.13.508.

- 1224 [38] G.Guralnik, C.R. Hagen and T.W.B. Kibble. “Global Conservation Laws and  
 1225 Massless Particles”. Physical Review Letters. 13 (20): 585–587, (1964). Bib-  
 1226 code:1964PhRvL..13..585G. doi:10.1103/PhysRevLett.13.585.
- 1227 [39] CMS collaboration. “Observation of a new boson at a mass of 125  
 1228 GeV with the CMS experiment at the LHC”. Physics Letters B.  
 1229 716 (1): 30–61 (2012). arXiv:1207.7235. Bibcode:2012PhLB..716...30C.  
 1230 doi:10.1016/j.physletb.2012.08.021
- 1231 [40] ATLAS collaboration. “Observation of a New Particle in the Search for the Stan-  
 1232 dard Model Higgs Boson with the ATLAS Detector at the LHC”. Physics Let-  
 1233 ters B. 716 (1): 1–29(2012). arXiv:1207.7214 Bibcode:2012PhLB..716....1A.  
 1234 doi:10.1016/j.physletb.2012.08.020.
- 1235 [41] ATLAS collaboration; CMS collaboration (26 March 2015). “Combined  
 1236 Measurement of the Higgs Boson Mass in pp Collisions at  $\sqrt{s}=7$  and  
 1237 8 TeV with the ATLAS and CMS Experiments”. Physical Review Let-  
 1238 ters. 114 (19): 191803. arXiv:1503.07589. Bibcode:2015PhRvL.114s1803A.  
 1239 doi:10.1103/PhysRevLett.114.191803.
- 1240 [42] CMS Collaboration, “SM Higgs Branching Ratios and To-  
 1241 tal Decay Widths (up-date in CERN Report4 2016)”.  
 1242 <https://twiki.cern.ch/twiki/bin/view/LHCPhysics/CERNYellowReportPageBR>, last accessed on 17.12.2017.
- 1244 [43] R.Grant V. “Determination of Higgs branching ratios in  $H \rightarrow W^+W^- \rightarrow l^+l^- jj$  and  $H \rightarrow ZZ \rightarrow l^+l^- jj$  channels”. Physics Department, Uni-  
 1245 versity of Tennessee (Dated: October 31, 2012). Retrieved from  
 1246 <http://aesop.phys.utk.edu/ph611/2012/projects/Riley.pdf>

- 1248 [44] LHC Higgs Cross Section Working Group, Denner, A., Heinemeyer, S. et al.  
 1249 “Standard model Higgs-boson branching ratios with uncertainties”. Eur. Phys.  
 1250 J. C (2011) 71: 1753. <https://doi.org/10.1140/epjc/s10052-011-1753-8>
- 1251 [45] LHC InternationalMasterclasses“When protons collide”. Retrieved from  
 1252 [http://atlas.physicsmasterclasses.org/en/zpath\\_protoncollisions.htm](http://atlas.physicsmasterclasses.org/en/zpath_protoncollisions.htm)
- 1253 [46] F. Maltoni, K. Paul, T. Stelzer, and S. Willenbrock, “Associated production  
 1254 of Higgs and single top at hadron colliders”, Phys.Rev. D64 (2001) 094023,  
 1255 [hep-ph/0106293].
- 1256 [47] S. Biswas, E. Gabrielli, F. Margaroli, and B. Mele, “Direct constraints on the  
 1257 top-Higgs coupling from the 8 TeV LHC data,” Journal of High Energy Physics,  
 1258 vol. 07, p. 073, (2013).
- 1259 [48] M. Farina, C. Grojean, F. Maltoni, E. Salvioni, and A. Thamm, “Lifting de-  
 1260 generacies in Higgs couplings using single top production in association with a  
 1261 Higgs boson,” Journal of High Energy Physics, vol. 05, p. 022, (2013).
- 1262 [49] T.M. Tait and C.-P. Yuan, “Single top quark production as a window to physics  
 1263 beyond the standard model”, Phys. Rev. D 63 (2000) 014018 [hep-ph/0007298].
- 1264 [50] F. Demartin, F. Maltoni, K. Mawatari, and M. Zaro, “Higgs production in  
 1265 association with a single top quark at the LHC,” European Physical Journal C,  
 1266 vol. 75, p. 267, (2015).
- 1267 [51] CMS Collaboration, “Modelling of the single top-quark pro-  
 1268 duction in association with the Higgs boson at 13 TeV.”  
 1269 <https://twiki.cern.ch/twiki/bin/viewauth/CMS/SingleTopHiggsGeneration13TeV>,  
 1270 last accessed on 16.01.2018.

- 1271 [52] CMS Collaboration, “SM Higgs production cross sections at  $\sqrt{s} = 13$  TeV.”  
 1272 <https://twiki.cern.ch/twiki/bin/view/LHCPhysics/CERNYellowReportPageAt13TeV>,  
 1273 last accessed on 16.01.2018.
- 1274 [53] S. Dawson, The effective W approximation, Nucl. Phys. B 249 (1985) 42.
- 1275 [54] S. Biswas, E. Gabrielli and B. Mele, JHEP 1301 (2013) 088 [arXiv:1211.0499  
 1276 [hep-ph]].
- 1277 [55] F. Demartin, B. Maier, F. Maltoni, K. Mawatari, and M. Zaro, “tWH associated  
 1278 production at the LHC”, European Physical Journal C, vol. 77, p. 34, (2017).  
 1279 arXiv:1607.05862
- 1280 [56] LHC Higgs Cross Section Working Group, “Handbook of LHC Higgs Cross  
 1281 Sections: 4.Deciphering the Nature of the Higgs Sector”, arXiv:1610.07922.
- 1282 [57] CMS Collaboration, “Search for the associated production of a Higgs boson  
 1283 with a single top quark in proton-proton collisions at  $\sqrt{s} = 8$  TeV”, JHEP 06  
 1284 (2016) 177, doi:10.1007/JHEP06(2016)177, arXiv:1509.08159.
- 1285 [58] B. Stieger, C. Jordá Lope et al., “Search for Associated Production of a Single  
 1286 Top Quark and a Higgs Boson in Leptonic Channels”, CMS Analysis Note CMS  
 1287 AN-14-140, 2014.
- 1288 [59] M. Peruzzi, C. Mueller, B. Stieger et al., “Search for ttH in multilepton final  
 1289 states at  $\sqrt{s} = 13$  TeV”, CMS Analysis Note CMS AN-16-211, 2016.
- 1290 [60] CMS Collaboration, “Search for H to bbar in association with a single top quark  
 1291 as a test of Higgs boson couplings at  $\sqrt{s} = 13$  TeV”, CMS Physics Analysis  
 1292 Summary CMS-PAS-HIG-16-019, 2016.

- 1293 [61] B. Maier, “SingleTopHiggProduction13TeV”, February, 2016.  
1294 <https://twiki.cern.ch/twiki/bin/viewauth/CMS/SingleTopHiggsGeneration13TeV>.
- 1295 [62] M. Peruzzi, F. Romeo, B. Stieger et al., “Search for ttH in multilepton final  
1296 states at  $\sqrt{s} = 13$  TeV”, CMS Analysis Note CMS AN-17-029, 2017.
- 1297 [63] B. WG, “BtagRecommendation80XReReco”, February, 2017.  
1298 <https://twiki.cern.ch/twiki/bin/view/CMS/BtagRecommendation80XReReco>.